

# Squared Wasserstein-2 Distance for Efficient Reconstruction of Stochastic Differential Equations

**Mingtao Xia\***

*Courant Institute of Mathematical Sciences  
New York University  
New York, NY 10012, USA*

XIAMINGTAO@NYU.EDU

**Xiangting Li\***

*Department of Computational Medicine  
University of California Los Angeles  
Los Angeles, CA 90095, USA*

XIANGTING.LI@UCLA.EDU

**Qijing Shen**

*Nuffield Department of Medicine  
University of Oxford  
Oxford OX2 6HW, UK*

QIJING.SHEN@NDM.OXFORD.EDU

**Tom Chou**

*Department of Mathematics,  
University of California Los Angeles  
Los Angeles, CA 90095, USA*

TOMCHOU@UCLA.EDU

## Abstract

We provide an analysis of the squared Wasserstein-2 ( $W_2$ ) distance between two probability distributions associated with two stochastic differential equations (SDEs). Based on this analysis, we propose the use of a squared  $W_2$  distance-based loss functions in the *reconstruction* of SDEs from noisy data. To demonstrate the practicality of our Wasserstein distance-based loss functions, we performed numerical experiments that demonstrate the efficiency of our method in reconstructing SDEs that arise across a number of applications.

**Keywords:** Wasserstein distance, stochastic differential equation, inverse problem, uncertainty quantification, optimal transport

## 1 Introduction

Stochastic processes are mathematical models of random phenomena that evolve over time or space (Cinlar, 2011). Among stochastic processes, stochastic differential equations (SDE) of the form

$$dX(t) = f(X(t), t)dt + \sigma(X(t), t)dB(t), \quad t \in [0, T] \quad (1)$$

---

\*. equal contribution

are widely used across different fields to model complex systems with continuous variables and noise. Here,  $f$  and  $\sigma$  denote deterministic and stochastic components of the SDE, while  $B(t)$  represents Brownian motion. In applications such as computational fluid dynamics, cell biology, and genetics, the underlying dynamics are often unknown, partially observed, and subjected to noise. Consequently, it is vital to develop methods capable of reconstructing the governing SDEs from limited data (Sullivan, 2015; Soize, 2017; Mathelin et al., 2005; Bressloff, 2014; Lin and Buchler, 2018). Traditional methods, such as the Kalman filter (Welch et al., 1995; Welch, 2020) and Gaussian process regression (Liu et al., 2020; MacKay et al., 1998) often assume specific forms of noise. These methods may not be suitable for complex or nonlinear systems where noise affects the dynamics in a more complex manner.

Recent advancements leverage machine learning, specifically neural ordinary differential equations (NODEs) (Chen et al., 2018), to offer a more flexible approach to reconstructing SDEs in the form of neural SDEs (nSDEs) (Tzen and Raginsky, 2019; Tong et al., 2022; Jia and Benson, 2019). Despite the promise, challenges remain, particularly in selecting optimal loss functions (Jia and Benson, 2019). The Wasserstein distance, a family of metrics that measures discrepancies between probability measures over a metric space, has emerged as a potential solution due to its robust properties (Villani et al., 2009; Oh et al., 2019; Zheng et al., 2020). In this paper, we introduce bounds on the second-order Wasserstein  $W_2$  distance between two probability distributions over the continuous function space generated by solutions to two SDEs. Our results motivate the use of this distance for SDE reconstruction. We test our approach on different examples to showcase its effectiveness.

Traditional methods for reconstructing SDEs from data usually make assumptions on the specific forms of the underlying SDE and fit unknown parameters. For example, (De Vecchi et al., 2016) uses some polynomials to model  $f, \sigma$ , while (Pereira et al., 2010) assumes linear  $f$  and  $\sigma$  in Eq. (1).

Previous attempts at using neural SDEs (nSDEs) have explored different loss functions for reconstruction. For example, Tzen and Raginsky (2019) model the SDE as a continuum limit of latent deep Gaussian models and use a variational likelihood bound for training. Kidger et al. (2021) adopt Wasserstein generative adversarial networks (WGANs) that were proposed in Arjovsky et al. (2017) for reconstructing SDEs. Briol et al. (2019) uses a maximum mean discrepancy (MMD) loss and a generative model for training SDEs. Song et al. (2020) assumes that  $\sigma$  in Eq. (1) depends only on time and uses a score-based generative model for SDE reconstruction.

The Wasserstein distance, denoted as  $W$ , has gained wide use in statistics and machine learning. Key papers have delved into its analysis (Rüschendorf, 1985) and its utilization in reconstructing discrete-time stochastic processes (Bartl et al., 2021). In the context of SDEs, Bion-Nadal and Talay (2019) introduced a restricted Wasserstein-type distance, while Sanz-Serna and Zygalkakis (2021) and Wang (2016); Sanz-Serna and Zygalkakis (2021) examined its application in ergodic SDEs, Levy processes, and Langevin equations, respec-

tively. Calculating the  $W$  distance for multidimensional random variables is challenging; hence, approximations such as the sliced  $W$  distance and regularized  $W$  distance have emerged (Cuturi et al., 2019; Kolouri et al., 2018, 2019; Rowland et al., 2019; Frogner et al., 2015).

The aforementioned WGAN approach in Kidger et al. (2021) uses the first-order Wasserstein distance to indirectly reconstruct SDEs via the Kantorovich-Rubinstein duality (Arjovsky et al., 2017). To the best of our knowledge, there has been no published work that directly applies and analyzes the  $W$  distance to the reconstruction of SDEs.

## 2 Definitions and Outline

We propose a squared  $W_2$ -distance-based SDE reconstruction method and analyze it under the following setting. Let  $\mu$  denote the probability distribution over the continuous function space  $C([0, T]; \mathbb{R})$  generated by the solution  $X(t)$  to Eq. (1). In the following approximation to Eq. (1),

$$d\hat{X}(t) = \hat{f}(X(t), t)dt + \hat{\sigma}(X(t), t)d\hat{B}(t), \quad t \in [0, T], \quad (2)$$

$\hat{B}(t)$  is another independent standard Brownian motion and the probability distribution over the continuous function space  $C([0, T]; \mathbb{R})$  generated by the solution  $\hat{X}(t)$  to Eq. (2) will be denoted  $\hat{\mu}$ .

We shall follow the definition of the squared  $W_2$ -distance in Clement and Desch (2008) for two probability measures  $\mu, \hat{\mu}$  associated with two continuous stochastic processes  $X(t), \hat{X}(t)$ ,  $t \in [0, T]$ .

**Definition 1** For two  $d$ -dimensional continuous stochastic processes in the separable space  $(C([0, T]; \mathbb{R}^d), \|\cdot\|)$

$$\mathbf{X}(t) = (X^1(t), \dots, X^d(t)), \quad \hat{\mathbf{X}}(t) = (\hat{X}^1(t), \dots, \hat{X}^d(t)), \quad t \in [0, T], \quad (3)$$

with two associated probability distributions  $\mu, \hat{\mu}$ , the squared  $W_2(\mu, \hat{\mu})$  distance between  $\mu, \hat{\mu}$  is defined as

$$W_2^2(\mu, \hat{\mu}) = \inf_{\pi(\mu, \hat{\mu})} \mathbb{E}_{(\mathbf{X}, \hat{\mathbf{X}}) \sim \pi(\mu, \hat{\mu})} [\|\mathbf{X} - \hat{\mathbf{X}}\|^2]. \quad (4)$$

The distance  $\|\mathbf{X}\| := \left(\int_0^T \sum_{i=1}^d |X_i(t)|^2 dt\right)^{\frac{1}{2}}$  and  $\pi(\mu, \hat{\mu})$  iterates over all *coupled* distributions of  $\mathbf{X}(t), \hat{\mathbf{X}}(t)$ , defined by the condition

$$\begin{cases} \mathbf{P}_{\pi(\mu, \hat{\mu})}(A \times C([0, T]; \mathbb{R}^d)) = \mathbf{P}_{\mu}(A), \\ \mathbf{P}_{\pi(\mu, \hat{\mu})}(C([0, T]; \mathbb{R}^d) \times A) = \mathbf{P}_{\hat{\mu}}(A), \end{cases} \quad \forall A \in \mathcal{B}(C([0, T]; \mathbb{R}^d)), \quad (5)$$

where  $\mathcal{B}(C([0, T]; \mathbb{R}^d))$  denotes the Borel  $\sigma$ -algebra associated with the space of  $d$ -dimensional continuous functions  $C([0, T]; \mathbb{R}^d)$ .

Our main contributions can be summarized as follows

1. Using Definition 1, we first derive in Section 3 an upper bound for the squared Wasserstein distance  $W_2^2(\mu, \hat{\mu})$  between the probability measures associated with solutions to two 1D SDEs in terms of the errors in the reconstructed drift and diffusion functions  $f - \hat{f}$  and  $\sigma - \hat{\sigma}$  in Eqs. (1) and (2). To be specific, we establish a  $W_2$  distance upper bound which depends explicitly on the difference in the drift and diffusion functions  $f - \hat{f}$  and  $\sigma - \hat{\sigma}$  associated with using Eq. (2) to approximate Eq. (1).
2. In Section 4, we shall prove that the  $W_2$  distance between the two SDEs,  $W_2(\mu, \hat{\mu})$ , can be accurately approximated by estimating the  $W_2$  distance between their finite-dimensional projections. We also develop a time-decoupled version of  $W_2^2(\mu, \hat{\mu})$  defined by

$$\tilde{W}_2^2(\mu, \hat{\mu}) := \int_0^T W_2^2(\mu(s), \hat{\mu}(s)) ds \quad (6)$$

which allows us to define a squared  $W_2$ -distance-based loss function for reconstructing SDEs. Here,  $\mu(s), \hat{\mu}(s)$  are the distributions on  $\mathbb{R}^d$  generated by projection of the stochastic processes  $\mathbf{X}, \hat{\mathbf{X}}$  at time  $s$ , respectively. Specifically, if  $X(t_i)$  follows a one-dimensional SDE Eq. (1), then for uniformly spaced time points  $t_i = \frac{iT}{N}$ ,  $i = 0, \dots, N$ , our proposed time-decoupled loss function is simply

$$\Delta t \sum_{i=1}^{N-1} \int_0^1 (F_i^{-1}(s) - \hat{F}_i^{-1}(s))^2 ds, \quad (7)$$

where  $\Delta t$  is the timestep and  $F_i$  and  $\hat{F}_i$  are the empirical cumulative distribution functions for  $X(t_i)$  and  $\hat{X}(t_i)$ , respectively. This time-decoupled squared  $W_2$ -distance loss function will be explicitly expressed in Eq. (18).

3. Finally, we carry out numerical experiments to show that our squared  $W_2$ -distance-based SDE reconstruction method performs better than recently developed machine-learning-based methods across many SDE reconstruction problems. In Section 6, we summarize our proposed squared  $W_2$  distance method for SDE reconstruction and suggest some promising future directions. Additional numerical experiments and sensitivity analysis are detailed in the Appendix.

### 3 Squared $W_2$ distance for reconstructing SDEs

In this section, we prove the bounds for the squared  $W_2$  distance of two probability measures associated with two SDEs. Specifically, we demonstrate that minimizing the squared  $W_2$  distance is necessary for the reconstruction of  $f, \sigma$  in Eq. (1).

We shall first prove an upper bound for the  $W_2$  distance between the probability measures  $\mu$  and  $\hat{\mu}$  associated with  $X(t), \hat{X}(t)$ , solutions to Eq. (1) and Eq. (2), respectively.

**Theorem 1** If  $\{X(t)\}_{t=0}^T, \{\hat{X}(t)\}_{t=0}^T$  have the same initial condition distribution and they are solutions to Eq. (1) and Eq. (2) in the univariate case ( $d = 1$  in Eq. (3)), respectively, and the following conditions hold:

- $f, \hat{f}, \sigma, \hat{\sigma}$  are continuously differentiable;  $\partial_x \sigma$  and  $\partial_x \hat{\sigma}$  are uniformly bounded
- there exists two functions  $\eta_1(x_1, x_2), \eta_2(x_1, x_2)$  such that their values are in  $(x_1, x_2)$  and

$$\begin{aligned} f(X_1, t) - f(X_2, t) &= \partial_x f(\eta_1(X_1, X_2), t)(X_1 - X_2) \\ \sigma(X_1, t) - \sigma(X_2, t) &= \partial_x \sigma(\eta_2(X_1, X_2), t)(X_1 - X_2) \end{aligned} \quad (8)$$

then,

$$\begin{aligned} W_2^2(\mu, \hat{\mu}) &\leq 3 \int_0^T \mathbb{E} \left[ \int_0^t H^2(s, t) ds \right] dt \times \mathbb{E} \left[ \int_0^T (f - \hat{f})^2(\tilde{X}(t), t) dt \right] \\ &\quad + 3 \int_0^T \mathbb{E} \left[ \int_0^t H^2(s, t) ds \right] dt \times \mathbb{E} \left[ \int_0^T (\partial_x \sigma(\eta_2(X(t), \tilde{X}(t)), t))^2 (\sigma - \hat{\sigma})^2(\tilde{X}(t), t) dt \right] \\ &\quad + 3 \int_0^T \mathbb{E} \left[ \int_0^t H^4(s, t) ds \right]^{1/2} dt \times \mathbb{E} \left[ \int_0^T (\sigma - \hat{\sigma})^4(\tilde{X}(t), t) dt \right]^{1/2}, \end{aligned} \quad (9)$$

where  $\tilde{X}(t)$  satisfies

$$d\tilde{X}(t) = \hat{f}(\tilde{X}(t), t)dt + \hat{\sigma}(\tilde{X}(t), t)dB(t), \quad \tilde{X}(0) = X(0), \quad (10)$$

and

$$H(s, t) := \exp \left[ \int_s^t h(X(r), \tilde{X}(r), r) dr + \int_s^t \partial_x \sigma(\eta_2(X(r), \tilde{X}(r), r)) dB(r) \right], \quad (11)$$

with  $h$  defined as

$$h(X(r), \tilde{X}(r), r) := \partial_x f(\eta_1(X(r), \tilde{X}(r)), r) - \left( \partial_x \sigma(\eta_2(X(r), \tilde{X}(r)), r) \right)^2. \quad (12)$$

The proof to Theorem 1 and its generalizations to higher dimensional stochastic dynamics under some specific assumptions are given in Appendix A. Theorem 1 indicates that as long as  $\mathbb{E} \left[ \int_0^t H^4(s, t) ds \right]$  is uniformly bounded for all  $t \in [0, T]$ , the upper bound for  $W_2(\mu, \hat{\mu}) \rightarrow 0$  when  $\hat{f} - f \rightarrow 0$  and  $\hat{\sigma} - \sigma \rightarrow 0$  uniformly in  $\mathbb{R} \times [0, T]$ . Specifically, if  $f = \hat{f}, \sigma = \hat{\sigma}$ , then the RHS Eq. (9) is 0. This means that minimizing  $W_2^2(\mu, \hat{\mu})$  is necessary for generating small errors  $\hat{f} - f, \hat{\sigma} - \sigma$  and for accurately approximating both  $f$  and  $\sigma$ . Thus, one can consider using the squared  $W_2$  distance as an effective loss function to minimize during reconstruction of SDEs. MSE-based loss functions (defined in Appendix E) suppress noise while the Kullback-Liebler (KL) divergence may not be finite, precluding resolution of  $X(t)$  and  $\hat{X}(t)$  even if  $\hat{f}$  approximates  $f$  and  $\hat{\sigma}$  approximates  $\sigma$ . Detailed discussions on the limitations of MSE and KL divergence in SDE reconstruction can be found in Appendix B.

#### 4 Finite-dimensional and time-decoupled squared $W_2$ loss functions

From Theorem 1 in Section 3, in order to have small errors in the drift and diffusion terms  $f - \hat{f}$  and  $\sigma - \hat{\sigma}$ , a small  $W_2(\mu, \hat{\mu})$  is necessary. However,  $W_2(\mu, \hat{\mu})$  cannot be directly used as a loss function to minimize since we cannot directly evaluate the integration in time in Eq. (4). In this section, we shall provide a way to estimate the  $W_2(\mu, \hat{\mu})$  distance by using finite dimensional projections, leading to squared  $W_2$ -distance-based loss functions for minimization.

Consider the two general  $d$ -dimensional SDEs defined in Eq. (41). Usually, we only have finite observations of trajectories for  $\{\mathbf{X}(t)\}$  and  $\{\hat{\mathbf{X}}(t)\}$  at discrete time points. Thus, we provide an estimate of the  $W_2$  between of the probability measures  $\mu, \hat{\mu}$  associated with  $\mathbf{X}(t)$  and  $\hat{\mathbf{X}}(t)$ ,  $t \in [0, T]$  using their finite-dimensional projections. We assume that  $\mathbf{X}(t), \hat{\mathbf{X}}(t)$  solve the two SDEs described by Eq. (41). We let  $0 = t_0 < t_1 < \dots < t_N = T, t_i = i\Delta t, \Delta t := \frac{T}{N}$  be a uniform mesh in time and we define the following projection operator  $\mathbf{I}_N$

$$\mathbf{X}_N(t) := \mathbf{I}_N \mathbf{X}(t) = \begin{cases} \mathbf{X}(t_i), t \in [t_i, t_{i+1}), i < N - 1, \\ \mathbf{X}(t_i), t \in [t_i, t_{i+1}), i = N - 1. \end{cases} \quad (13)$$

As in the previous case, we require  $\mathbf{X}(t)$  and  $\hat{\mathbf{X}}(t)$  to be continuous. Note that the projected process is no longer continuous. Thus, we define a new space  $\tilde{\Omega}_N$  containing all continuous and piecewise constant functions; naturally,  $\mu, \hat{\mu}$  are allowed to be defined on  $\tilde{\Omega}_N$ . Distributions over  $\tilde{\Omega}_N$  generated by  $\mathbf{X}_N(t), \hat{\mathbf{X}}_N(t)$  in Eq. (13) is denoted by  $\mu_N$  and  $\hat{\mu}_N$ , respectively. We will prove the following theorem for estimating  $W_2(\mu, \hat{\mu})$  by  $W_2(\mu_N, \hat{\mu}_N)$ .

**Theorem 2** Suppose  $\{\mathbf{X}(t)\}_{t=0}^T$  and  $\{\hat{\mathbf{X}}(t)\}_{t=0}^T$  are both continuous-time continuous-space stochastic processes in  $\mathbb{R}^d$  and  $\mu, \hat{\mu}$  are their associated probability measures, then  $W_2(\mu, \hat{\mu})$  can be bounded by their finite-dimensional projections

$$W_2(\mu_N, \hat{\mu}_N) - W_2(\mu, \mu_N) - W_2(\hat{\mu}, \hat{\mu}_N) \leq W_2(\mu, \hat{\mu}) \leq W_2(\mu_N, \hat{\mu}_N) + W_2(\mu, \mu_N) + W_2(\hat{\mu}, \hat{\mu}_N) \quad (14)$$

where  $\mu_N, \hat{\mu}_N$  are the probability distributions associated with  $\mathbf{X}_N$  and  $\hat{\mathbf{X}}_N$  defined in Eq. (13). Specifically, if  $\mathbf{X}(t)$  and  $\hat{\mathbf{X}}(t)$  solve Eq. (41), and if

$$\begin{aligned} F &:= \mathbb{E} \left[ \int_0^T \sum_{i=1}^d f_i^2(\mathbf{X}(t), t) dt \right] < \infty, \quad \Sigma := \mathbb{E} \left[ \int_0^T \sum_{\ell=1}^d \sum_{j=1}^s \sigma_{\ell, j}^2(\mathbf{X}(t), t) dt \right] < \infty, \\ \hat{F} &:= \mathbb{E} \left[ \int_0^T \sum_{i=1}^d \hat{f}_i^2(\hat{\mathbf{X}}(t), t) dt \right] < \infty, \quad \hat{\Sigma} := \mathbb{E} \left[ \int_0^T \sum_{\ell=1}^d \sum_{j=1}^s \hat{\sigma}_{\ell, j}^2(\hat{\mathbf{X}}(t), t) dt \right] < \infty, \end{aligned} \quad (15)$$

then we obtain the following bound

$$\begin{aligned} W_2(\mu_N, \hat{\mu}_N) - \sqrt{(s+1)\Delta t} \left( \sqrt{F\Delta t + \Sigma} + \sqrt{\hat{F}\Delta t + \hat{\Sigma}} \right) &\leq W_2(\mu, \hat{\mu}) \\ &\leq W_2(\mu_N, \hat{\mu}_N) + \sqrt{(s+1)\Delta t} \left( \sqrt{F\Delta t + \Sigma} + \sqrt{\hat{F}\Delta t + \hat{\Sigma}} \right). \end{aligned} \quad (16)$$

The proof to Theorem 2 relies on the triangular inequality of the Wasserstein distance and the Itô isometry; it is provided in Appendix C. Theorem 2 gives bounds for approximating the  $W_2$  distance between  $\mathbf{X}(t), \hat{\mathbf{X}}(t)$  w.r.t. to their finite dimensional projections  $\mathbf{X}_N(t), \hat{\mathbf{X}}_N(t)$ . Specifically, if  $\mathbf{X}(t), \hat{\mathbf{X}}(t)$  are solutions to Eq. (1) and Eq. (2), then as the timestep  $\Delta t \rightarrow 0$ ,  $W_2(\mu_N, \hat{\mu}_N) \rightarrow W_2(\mu, \hat{\mu})$ . Theorem 2 indicates that we can use  $W_2^2(\mu_N, \hat{\mu}_N)$ , which approximates  $W_2^2(\mu, \hat{\mu})$  when  $\Delta t \rightarrow 0$ , as a loss function. Furthermore,

$$W_2^2(\mu_N, \hat{\mu}_N) = \inf_{\pi(\mu_N, \hat{\mu}_N)} \sum_{i=1}^{N-1} \mathbb{E}_{(\mathbf{X}_N, \hat{\mathbf{X}}_N) \sim \pi(\mu_N, \hat{\mu}_N)} \left[ \|\mathbf{X}(t_i) - \hat{\mathbf{X}}(t_i)\|_2^2 \right] \Delta t. \quad (17)$$

Here,  $\pi(\mu_N, \hat{\mu}_N)$  iterates over coupled distributions of  $\mathbf{X}_N(t), \hat{\mathbf{X}}_N(t)$ , whose marginal distributions coincide with  $\mu_N$  and  $\hat{\mu}_N$ .  $\|\cdot\|_2$  denotes the  $\ell^2$  norm of a vector. Note that  $\mu_N$  is fully characterized by values of  $\mathbf{X}(t)$  at the discrete time points  $t_i$ .

For a  $d$ -dimensional SDE, the trajectories at discrete time points  $\{\mathbf{X}(t_i)\}_{i=1}^{N-1}$  is  $d \times (N-1)$  dimensional. In Fournier and Guillin (2015), the error bound for  $|W_2^2(\mu_N, \hat{\mu}_N) - W_2^2(\mu_N^e, \hat{\mu}_N^e)|$ , where  $\mu_N^e, \hat{\mu}_N^e$  are the finite-sample empirical distributions of  $\{\mathbf{X}(t_i)\}_{i=1}^{N-1}$  and  $\{\hat{\mathbf{X}}(t_i)\}_{i=1}^{N-1}$ , will increase as the dimensionality  $d \times (N-1)$  becomes large. Alternatively, we can disregard the temporal correlations of values at different times and relax the constraint on the coupling  $\pi(\mu_N, \hat{\mu}_N)$  in to minimize the Wasserstein distance between the marginal distribution of  $\{\mathbf{X}(t_i)\}$  and the marginal distribution of  $\{\hat{\mathbf{X}}(t_i)\}$ , as was done in Chewi et al. (2021). To be more specific, we minimize individual terms in the sum with respect to the coupling  $\pi_i$  of  $\mathbf{X}(t_i)$  and  $\hat{\mathbf{X}}(t_i)$  and define a heuristic loss function

$$\sum_{i=1}^{N-1} \inf_{\pi_i} \mathbb{E}_{\pi_i} \left[ \|\mathbf{X}(t_i) - \hat{\mathbf{X}}(t_i)\|_2^2 \right] \Delta t = \sum_{i=1}^{N-1} W_2^2(\mu_N(t_i), \hat{\mu}_N(t_i)) \Delta t \quad (18)$$

where  $\mu_N(t)$  and  $\hat{\mu}_N(t)$  are the probability distributions of  $\mathbf{X}(t)$  and  $\hat{\mathbf{X}}(t)$ , respectively. Note that

$$\sum_{i=1}^{N-1} \inf_{\pi_i} \mathbb{E}_{\pi_i} \left[ \|\mathbf{X}(t_i) - \hat{\mathbf{X}}(t_i)\|_2^2 \right] \Delta t \leq W_2^2(\mu_N, \hat{\mu}_N) \quad (19)$$

because the marginal distributions of  $\pi(\mu_N, \hat{\mu}_N)$  coincide with  $\mu_N$  and  $\hat{\mu}_N$ . Since the marginal distributions of  $\mu_N$  and  $\hat{\mu}_N$  at  $t_i$  are  $\mu_N(t_i)$  and  $\hat{\mu}_N(t_i)$ , respectively, we have

$$\begin{aligned}
 & \sum_{i=1}^{N-1} \inf_{\pi_i} \mathbb{E}_{\pi_i} \left[ \|\mathbf{X}(t_i) - \hat{\mathbf{X}}(t_i)\|_2^2 \right] \Delta t \\
 & \leq \inf_{\pi(\mu_N, \hat{\mu}_N)} \sum_{i=1}^{N-1} \mathbb{E}_{(\mathbf{X}_N, \hat{\mathbf{X}}_N) \sim \pi(\mu_N, \hat{\mu}_N)} \left[ \|\mathbf{X}(t_i) - \hat{\mathbf{X}}(t_i)\|_2^2 \right] \Delta t.
 \end{aligned} \tag{20}$$

The dimensionality of  $\mathbf{X}(t_i)$  and  $\hat{\mathbf{X}}(t_i)$  is  $d$ , which is much smaller than  $(N-1)d$  for large  $N$ . We denote  $\mu_N^e(t_i)$  and  $\hat{\mu}_N^e(t_i)$  to be the finite-sample empirical distributions of  $\mathbf{X}(t_i)$  and  $\hat{\mathbf{X}}(t_i)$ , respectively. Since the error of estimating the  $W_2$  distance using empirical distributions of a random variable increases with the random variable's dimensionality Fournier and Guillin (2015), the error  $\left| \sum_{i=1}^{N-1} W_2^2(\mu_N(t_i), \hat{\mu}_N(t_i)) - \sum_{i=1}^{N-1} W_2^2(\mu_N^e(t_i), \hat{\mu}_N^e(t_i)) \right|$  can be smaller than the error  $|W_2^2(\mu_N, \hat{\mu}_N) - W_2^2(\mu_N^e, \hat{\mu}_N^e)|$ . Compared to Eq. (17), the time-decoupled squared  $W_2$  distance Eq. (18) can be better approximated using finite-sample empirical distributions.

Note that

$$\sum_{i=1}^{N-1} W_2^2(\mu_N(t_i), \hat{\mu}_N(t_i)) \Delta t \leq W_2^2(\mu_N, \hat{\mu}_N). \tag{21}$$

Thus, from Theorem 1 and Theorem 2, minimizing Eq. (18) when  $N \rightarrow \infty$  is also necessary to achieve small  $f - \hat{f}$  and  $\sigma - \hat{\sigma}$  when the SDE is univariate. Let  $\mu_i, \hat{\mu}_i$  be the two probability distributions on the space of continuous functions associated with  $\mathbf{X}(t), t \in [t_i, t_{i+1})$  and  $\hat{\mathbf{X}}(t), t \in [t_i, t_{i+1})$ , respectively. We can then show that Eq. (18) is an approximation to the partially time-decoupled summation of squared  $W_2$  distances  $\sum_{i=1}^{N-1} W_2^2(\mu_i, \hat{\mu}_i)$  as  $N \rightarrow \infty$ . Additionally, we can prove the following theorem that indicates Eq. (18) approximates a time-decoupled squared Wasserstein distance in the  $N \rightarrow \infty$  limit.

**Theorem 3** We assume the conditions in Theorem 2 hold and for any  $0 < t < t' < T$ , as  $t' - t \rightarrow 0$ , the following conditions are satisfied

$$\begin{aligned}
 & \mathbb{E} \left[ \int_t^{t'} \sum_{i=1}^d f_i^2(\mathbf{X}(t), t) dt \right], \mathbb{E} \left[ \int_t^{t'} \sum_{i=1}^d \hat{f}_i^2(\hat{\mathbf{X}}(t), t) dt \right] \rightarrow 0, \\
 & \mathbb{E} \left[ \int_t^{t'} \sum_{i=1}^d \sum_{j=1}^s \sigma_{i,j}^2(\mathbf{X}(t), t) dt \right], \mathbb{E} \left[ \int_t^{t'} \sum_{i=1}^d \sum_{j=1}^s \hat{\sigma}_{i,j}^2(\hat{\mathbf{X}}(t), t) dt \right] \rightarrow 0.
 \end{aligned} \tag{22}$$

Then,

$$\lim_{N \rightarrow \infty} \left( \sum_{i=1}^{N-1} \inf_{\pi_i} \mathbb{E}_{\pi_i} \left[ \|\mathbf{X}(t_i) - \hat{\mathbf{X}}(t_i)\|_2^2 \right] \Delta t - \sum_{i=1}^{N-1} W_2^2(\mu_i, \hat{\mu}_i) \right) = 0. \tag{23}$$

Furthermore, the limit

$$\lim_{N \rightarrow \infty} \sum_{i=1}^{N-1} \inf_{\pi_i} \mathbb{E}_{\pi_i} \left[ |\mathbf{X}(t_i) - \hat{\mathbf{X}}(t_i)|_2^2 \right] \Delta t = \lim_{N \rightarrow \infty} \sum_{i=1}^{N-1} W_2^2(\mu(t_i), \hat{\mu}(t_i)) \Delta t \quad (24)$$

exists.

The proof of Theorem 3 will use the result of Theorem 2 and is given in Appendix D. Specifically, for each  $N$ ,

$$\sum_{i=1}^{N-1} \inf_{\pi_i} \mathbb{E}_{\pi_i} \left[ |\mathbf{X}(t_i) - \hat{\mathbf{X}}(t_i)|_2^2 \right] \Delta t \leq W_2^2(\mu_N, \hat{\mu}_N), \quad (25)$$

so we conclude that

$$\lim_{N \rightarrow \infty} \sum_{i=1}^{N-1} \inf_{\pi_i} \mathbb{E}_{\pi_i} \left[ |\mathbf{X}(t_i) - \hat{\mathbf{X}}(t_i)|_2^2 \right] \Delta t \leq \lim_{N \rightarrow \infty} W_2^2(\mu_N, \hat{\mu}_N) = W_2^2(\mu, \hat{\mu}). \quad (26)$$

We denote

$$\tilde{W}_2^2(\mu, \hat{\mu}) := \int_0^T W_2^2(\mu(t), \hat{\mu}(t)) dt = \lim_{N \rightarrow \infty} \sum_{i=1}^{N-1} W_2^2(\mu(t_i^1), \hat{\mu}(t_i^1)) (t_i^1 - t_{i-1}^1) \quad (27)$$

as the *time-decoupled squared Wasserstein distance*. From Eq. (26), we can deduce that

$$\tilde{W}_2^2(\mu, \hat{\mu}) \leq W_2^2(\mu, \hat{\mu}). \quad (28)$$

Therefore, the upper bound of  $W_2^2(\mu, \hat{\mu})$  in Theorem 1 is also an upper bound of  $\tilde{W}_2^2(\mu, \hat{\mu})$ , *i.e.*, to reconstruct a 1D SDE by minimizing  $\tilde{W}_2^2(\mu, \hat{\mu})$ , it is necessary that  $f - \hat{f}$  and  $\sigma - \hat{\sigma}$  are small. From Theorem 3, minimizing the finite-time-point time-decoupled loss function defined in Eq. (18), which approximates  $\tilde{W}_2^2(\mu, \hat{\mu})$  when  $\Delta t$  is small, is needed for minimizing  $f - \hat{f}$  and  $\sigma - \hat{\sigma}$ .

Specifically, if  $X(t), \hat{X}(t)$  are solutions to the univariate SDEs Eq. (1) and Eq. (2), then Eq. (18) reduces to Eq. (7), which can be directly calculated. In Example 3, Example 4, and Appendix J, we shall compare use of the two different squared  $W_2$  distance loss functions Eqs. (17) and (18). From our preliminary numerical results, using Eq. (18) is more efficient than using Eq. (17) and gives more accurate reconstructed SDEs.

## 5 Numerical experiments

We carry out experiments to investigate the efficiency of our proposed squared  $W_2$  loss function (Eq. (18)) by comparing it to other methods and loss functions. Our approach is tested on the reconstruction of several representative SDEs in Examples 1– 4.

In all experiments, we use two neural networks to parameterize  $\hat{f} := \hat{f}(X, t; \Theta_1), \hat{\sigma} := \hat{\sigma}(X, t; \Theta_2)$  in Eq. (2) for the purpose of reconstructing  $f, \sigma$  in Eq. (1) by the estimates

$\hat{f} \approx f, \hat{\sigma} \approx \sigma$ .  $\Theta_1, \Theta_2$  are the parameter sets in the two neural networks for parameterizing  $\hat{f} = \hat{f}_{\Theta_1}, \hat{\sigma} = \hat{\sigma}_{\Theta_2}$ . We use the `sdeint` function in the `torchsde` Python package in Li et al. (2020) to numerically integrate SDEs. Details of the training hyperparameter setting for all examples are given in Appendix F. Our code will be made publicly available on Github upon acceptance of this manuscript.

First, we compare our proposed squared  $W_2$ -distance-based loss (Eq. (18)) with several traditional statistical methods for SDE reconstruction.

**Example 1** We reconstruct a nonlinear SDE of the form

$$dX(t) = \left(\frac{1}{2} - \cos X(t)\right)dt + \sigma dB(t), \quad t \in [0, 20], \quad (29)$$

which defines a Brownian process in a potential of the form  $U(x) = \frac{x}{2} - \sin x$ . In the absence of noise, there are infinitely many stable equilibrium points  $x_k = \frac{5\pi}{3} + 2\pi k, k \in \mathbb{Z}$ . When noise  $\sigma dB(t)$  is added, trajectories tend to saturate around those equilibrium points but jumping from one equilibrium point to another is possible. We use the MSE, the mean<sup>2</sup>+variance, the maximum-log-likelihood, and the proposed finite-time-point time-decoupled squared  $W_2$  distance Eq. (18) as loss functions to reconstruct Eq. (29). For all loss functions, we use the same neural network hyperparameters. Definitions of all loss functions and training details are provided in Appendix E. As detailed in Appendix F, neural networks with the same number of hidden layers and neurons in each layer are used for each loss function. Using the initial condition  $X(0) = 0$ , the sampled ground-truth and reconstructed trajectories are shown in Fig. 1.

Fig. 1(a) shows the distributions of 100 trajectories with most of them concentrated around two attractors (local minima  $x = -\frac{\pi}{3}, \frac{5\pi}{3}$  of the potential  $U(x)$ ). Fig. 1(b) shows that using MSE gives almost deterministic trajectories and fails to reconstruct the noise. From 1(c), we see that the mean<sup>2</sup>+variance loss fails to reconstruct the two local equilibria because cannot sufficiently resolve the shape of the trajectory distribution at any fixed timepoint. Fig. 1(d) shows that when using our proposed finite-time-point time-decoupled squared  $W_2$  loss Eq. (18), the trajectories of the reconstructed SDE can successfully learn the two-attractor feature and potentially the distribution of trajectories. The reason why the reconstructed trajectories of the  $W_2$  distance cannot recover the third stable equilibrium at  $x = \frac{11\pi}{3}$  is because the data is sparse near it. From 1(e), we see that the max-log-likelihood loss performs the worst as it yields almost the same curves for all realizations.

In the next example, we show how using our finite-time-point time-decoupled squared  $W_2$  distance loss function Eq. (18) can lead to efficient reconstruction of  $f$  and  $\sigma$ . We shall use the mean relative  $L^2$  error

$$\left( \frac{\sum_{i=0}^T \sum_{j=1}^N \|f(x_j(t_i), t_i) - \hat{f}(x_j(t_i), t_i)\|^2}{(T+1) \sum_{j=1}^N \|f(x_j(t_i), t_i)\|^2} \right)^{\frac{1}{2}}, \quad \left( \frac{\sum_{i=0}^T \sum_{j=1}^N \left| \|\sigma(x_j(t_i), t_i)\| - \|\hat{\sigma}(x_j(t_i), t_i)\| \right|^2}{(T+1) \sum_{j=1}^N \|\sigma(x_j(t_i), t_i)\|^2} \right)^{\frac{1}{2}} \quad (30)$$

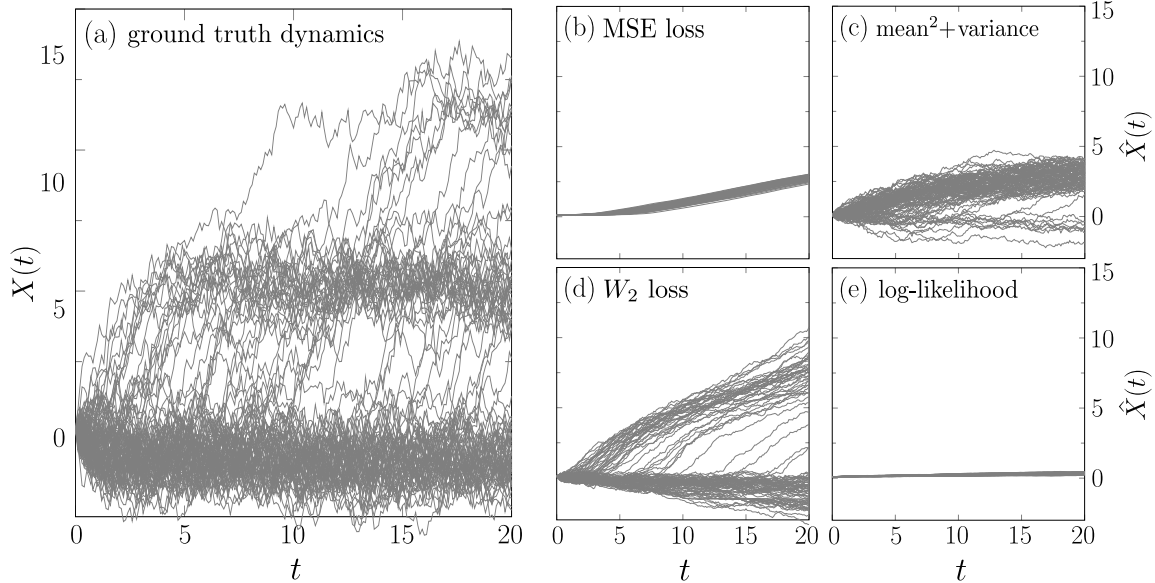


Figure 1: (a) Ground-truth trajectories. (b) Reconstructed trajectories from nSDE using MSE loss. (c) Reconstructed trajectories from nSDE using  $\text{mean}^2 + \text{variance}$  loss. (d) Reconstructed trajectories from nSDE using the finite-time-point time-decoupled  $W_2$  loss. (e) Reconstructed trajectories from nSDE using a max-log-likelihood loss yields the worst approximation.

between the reconstructed  $\hat{f}, \hat{\sigma}$  in Eq. (2) and the ground-truth  $f$  and  $\sigma$  in Eq. (1). Here,  $x_j(t_i)$  is the value of the  $j^{\text{th}}$  ground-truth trajectory at  $t_i$ .

**Example 2** Next, we reconstruct a Cox-Ingersoll-Ross (CIR) model which is a popular finance model that describes the evolution of interest rates:

$$dX(t) = (5 - X(t))dt + \sigma_0 \sqrt{X(t)}dB(t), \quad t \in [0, 2]. \quad (31)$$

Specifically, we are interested in how our reconstructed  $\hat{f}, \hat{\sigma}$  can approximate the ground-truth  $f(X) = 5 - X$  and  $\sigma(X) = \sigma_0 \sqrt{X}$  (with  $\sigma_0$  a constant parameter). Here, we take the timestep  $\Delta t = 0.05$  in Eq. (18) and the initial condition is  $X(0) = 2$ . For reconstructing  $f$  and  $\sigma$ , we compare using our proposed finite-time-point time-decoupled squared  $W_2$  distance Eq. (18) with minimizing a Maximum Mean Discrepancy (MMD) (Briol et al., 2019) and other loss functions given in Appendix E. Hyperparameters in the neural networks used for training are the same across all loss functions.

Fig. 2(a) shows the predicted trajectories using our proposed squared  $W_2$  loss function match well with the ground-truth trajectories. Fig. 2(b, c) indicate that, if  $\gtrsim 100$  ground-truth trajectories are used, our proposed squared  $W_2$  distance loss yields smaller errors in

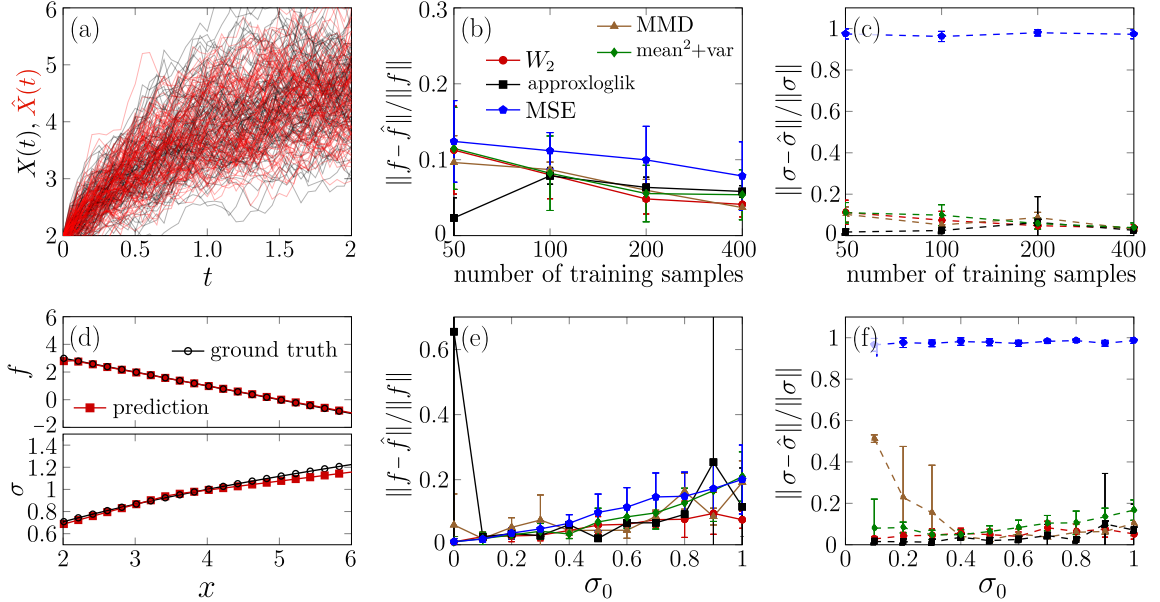


Figure 2: (a) Ground-truth trajectories and reconstructed trajectories by nSDE using the finite-time-point time-decoupled squared  $W_2$  loss with  $\sigma_0 = 0.5$ . (b-c) Errors with respect to the numbers of ground-truth trajectories for  $\sigma_0 = 0.5$ . (d) Comparison of the reconstructed  $\hat{f}_{\Theta_1}(u), \hat{\sigma}_{\Theta_2}(u)$  to the ground-truth functions  $f(u), \sigma(u)$  for  $\sigma_0 = 0.5$ . (e-f) Errors with respect to noise level  $\sigma_0$  with 200 training samples. Legends for panels (c, e, f) are the same as the one in (b).

$f, \sigma$  as defined in Eq. (30). More specifically, we plot the reconstructed  $\hat{f}_{\Theta}, \hat{\sigma}_{\Theta}$  by using our squared  $W_2$  loss in Fig. 2(d); these reconstructions also match well with the ground-truth values  $f, \sigma$ . When we vary  $\sigma_0$  in Eq. (31), our proposed finite-time-point time-decoupled  $W_2$  loss function gives the best performance among all loss functions shown in Fig. 2(e, f). In Appendix G, instead of using the same initial condition for all trajectories, we sample the initial condition from different distributions and find that the reconstruction errors  $f - \hat{f}$  and  $\sigma - \hat{\sigma}$  is **not** sensitive to different initial conditions, implying the robustness of using our proposed finite-time-point time-decoupled  $W_2$  loss function with respect to different initial conditions. Also, in Appendix H, we change the number of layers and the number of neurons in each layers for the two neural networks we utilize to parameterize  $\hat{f} := \hat{f}(X, t; \Theta_1), \hat{\sigma} := \hat{\sigma}(X, t; \Theta_2)$ . We find that wider neural networks can lead to smaller errors  $f - \hat{f}$  and  $\sigma - \hat{\sigma}$ .

Next, we reconstruct the Ornstein-Uhlenbeck (OU) process given in Kidger et al. (2021) and in doing so, compare our loss function with the WGAN-SDE method therein and with another recent MMD method.

**Example 3** Consider reconstructing the following time-inhomogeneous OU process

$$dX(t) = (0.02t - 0.1X(t))dt + 0.4dB(t), \quad t \in [0, 63]. \quad (32)$$

We compare the numerical performance of minimizing Eq. (17) or minimizing Eq. (18) with the WGAN method and using the MMD loss metric. Eq. (17) is numerically evaluated using the `ot.emd2` function in the Python Optimal Transport package (Flamary et al., 2021) We take the timestep  $\Delta t = 1$  in Eq. (18) and Eq. (17) and the initial condition is taken as  $X(0) = 0$ . Neural networks with the same number of hidden layers and neurons in each layer are used for all three methods (see Appendix F).

In addition to the relative error in the reconstructed  $\hat{f}, \hat{\sigma}$ , we also compare the runtime and memory usage used by the three methods as a function of the number of ground-truth trajectories used in training. From Fig. 3(a), the distribution of trajectories of the

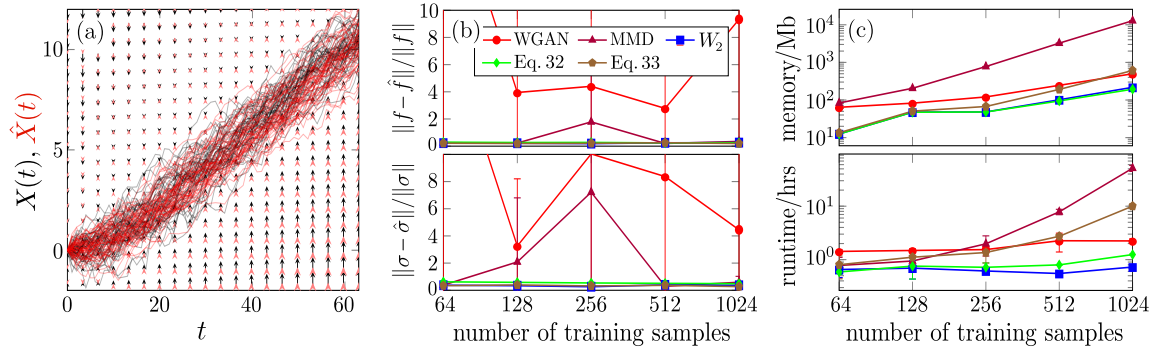


Figure 3: (a) Ground-truth and reconstructed trajectories using the squared  $W_2$  loss Eq. (18). Black and red curves are ground-truth and reconstructed trajectories, respectively. Black and red arrows indicate  $f(x, t)$  and the reconstructed  $\hat{f}(x, t)$  at fixed  $(x, t)$ , respectively. (b) Relative errors in reconstructed  $\hat{f}$  and  $\hat{\sigma}$ , repeated 10 times. Error bars show the standard deviation. (c) Resource consumption with respect to the number of training samples  $N_{\text{samples}}$ . Memory usage is measured by torch profiler and represents peak memory usage during training. The legend in the panel (c) is the same as the one in (b).

reconstructed SDE found from using our proposed squared  $W_2$  loss Eq. (18) matches well with the distribution of the ground-truth trajectories. Both minimizing Eq. (17) and minimizing Eq. (18) outperform the other two methods in the relative  $L^2$  error of the

reconstructed  $f, \sigma$  for all numbers of ground-truth trajectories. Using Eq. (18) as the loss function achieves better accuracy in a shorter computational time than using Eq. (17).

For  $N_{\text{sample}}$  training samples and  $N$  total number of timesteps, the memory cost in using Eq. (18) is  $O(N \times N_{\text{sample}})$ ; however, the number of operations needed is  $O(N \times N_{\text{sample}} \log N_{\text{sample}})$  because we need to reorder the ground-truth  $X(t_i)$  and predicted  $\hat{X}(t_i)$  data to obtain the empirical cumulative distributions at every  $t_i$ . The memory cost and operations needed in using Eq. (17) are both  $O((N \times N_{\text{sample}})^2)$  because a  $(N \times N_{\text{sample}}) \times (N \times N_{\text{sample}})$  cost matrix must be evaluated. On the other hand, the MMD method needs to create an  $N_{\text{sample}} \times N_{\text{sample}}$  matrix for each timestep and thus the corresponding memory cost and operations needed are at best  $O(N \times N_{\text{sample}}^2)$ . The WGAN-SDE method needs to create a generator and a discriminator and its training is complex, leading to both a higher memory cost and a larger runtime than our method. For reconstructing SDEs, a larger number of ground-truth trajectories leads to higher accuracy (see Appendix I). Overall, our time-decoupled squared  $W_2$  loss, Eq. (18), performs the best in terms of accuracy and efficiency when reconstructing the 1D SDE Eq. (32).

If we consider using stochastic gradient descent (SDG) to minibatch for training, we find that the batch size cannot be set too small, especially when we are using the MMD or Eq. (17) as loss functions, due to the intrinsic noisy nature of trajectories of SDEs. Thus, using our squared  $W_2$  distance loss function given in Eq. (18) can be more efficient overall than using the MMD or Eq. (17) as the loss function. Additional results using the SGD with minibatch for training are given in Appendix I.

Finally, we carry out an experiment on reconstructing a 2D correlated geometric Brownian motion. In this 2D reconstruction problem, we will compare the loss functions, Eq. (17) and Eq. (18), the MMD method, and a sliced squared Wasserstein distance method (Kolouri et al., 2018).

**Example 4** Consider reconstructing the following 2D correlated geometric Brownian motion that can represent, *e.g.*, values of two correlated stocks (Musielà and Rutkowski, 2006)

$$\begin{aligned} dX_1(t) &= \mu_1 X_1(t) dt + \sum_{i=1}^2 \sigma_{1,i} X_i(t) dB_i(t), \\ dX_2(t) &= \mu_2 X_2(t) dt + \sum_{i=1}^2 \sigma_{2,i} X_i(t) dB_i(t) \end{aligned} \tag{33}$$

Here,  $t \in [0, 2]$ ,  $B_1(t)$  and  $B_2(t)$  are independent Brownian processes,  $\mathbf{f} := (\mu_1 X_1, \mu_2 X_2)$  is a 2D vector, and  $\boldsymbol{\sigma} := [\sigma_{1,1} X_1, \sigma_{1,2} X_2; \sigma_{2,1} X_1, \sigma_{2,2} X_2]$  is a  $2 \times 2$  matrix. We use  $(\mu_1, \mu_2) = (0.1, 0.2)$ ,  $\boldsymbol{\sigma} = [0.2X_1, -0.1X_2; -0.1X_1, 0.1X_2]$ , and set the initial condition  $(X_1(0), X_2(0)) = (1, 0.5)$ . In addition to directly minimizing a 2D decorrelated version of the squared  $W_2$  distance Eq. (18) (denoted as  $W_2$  in Fig. 4(c)), we consider minimizing

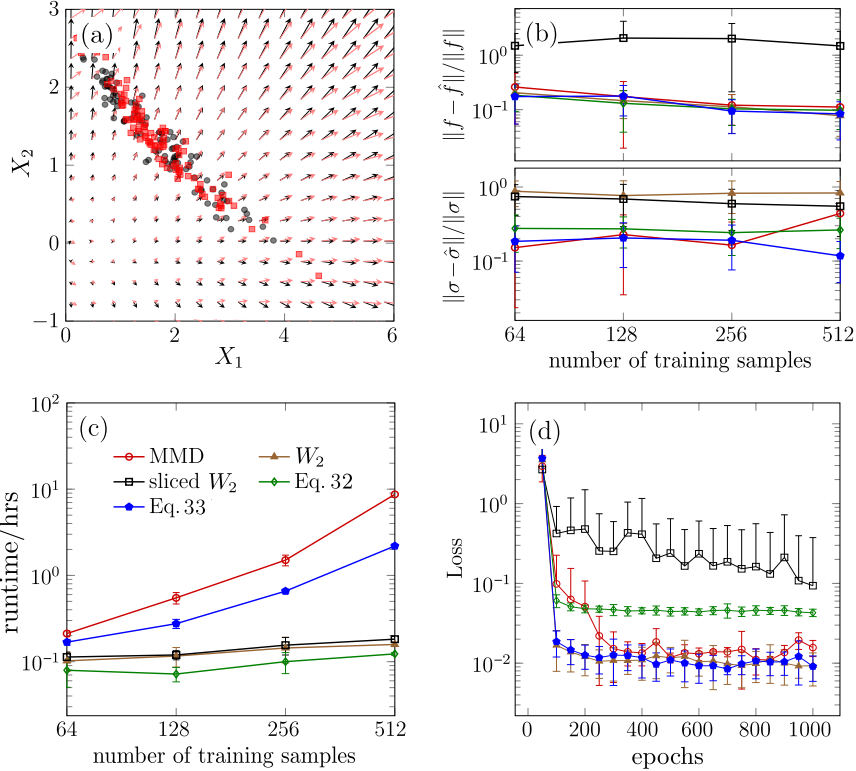


Figure 4: (a) Black dots and red squares are the ground-truth  $(X_1(2), X_2(2))$  and the reconstructed  $(\hat{X}_1(2), \hat{X}_2(2))$  found using the rotated squared  $W_2$  loss function, respectively. Black and red arrows indicate, respectively, the vectors  $\mathbf{f}(X_1, X_2)$  and  $\hat{\mathbf{f}}(X_1, X_2)$ . (b) Relative errors of the reconstructed  $\mathbf{f}$  and  $\sigma$ . Error bars indicate the standard deviation across ten reconstructions. (c) Runtime of different loss functions with respect to  $N_{\text{samples}}$ . (d) The decrease of different loss functions with respect to training epochs. The legend for the panel (d) is the same as the one in (c).

a sliced squared  $W_2$  distance as proposed by Kolouri et al. (2018, 2019). Finally, we numerically estimate the  $W_2$  distance Eq. (17) as well as the time-decoupled approximation Eq. (18) using the `ot.emd2` function in the Python Optimal Transport package. Formulae of the above loss functions are given in Appendix E. We keep the neural network hyperparameters the same while minimizing all loss functions. Note that since the SDE has two components, the definition of the relative error in  $\sigma$  is revised to

$$\left[ \frac{\sum_{i=0}^T \sum_{j=1}^N \|\sigma\sigma^T(x_j(t_i), t_i) - \hat{\sigma}\hat{\sigma}^T(x_j(t_i), t_i)\|_F^2}{(T+1) \sum_{j=1}^N \|\hat{\sigma}\hat{\sigma}^T(x_j(t_i), t_i)\|_F^2} \right]^{1/2}, \quad (34)$$

where  $\|\cdot\|_F$  is the Frobenius norm for matrices.

Fig. 4(a) shows the ground truth and reconstructed coordinates  $(X_1, X_2)$  (black dots) and  $(\hat{X}_1, \hat{X}_2)$  (red squares) at time  $t = 2$ , along with  $\mathbf{f}(X_1, X_2)$  (black) and  $\hat{\mathbf{f}}(X_1, X_2)$  (red). For reconstructing  $\mathbf{f}$  and  $\sigma$  in problem, numerically evaluating Eq. (18) (blue curve) performs better than the MMD method, the loss in Eq. (17), the sliced  $W_2$  distance loss, and the 2D decorrelated squared  $W_2$  loss, as shown in Fig. 4(b). Using the sliced  $W_2$  distance yields the poorest performance and least accurate  $\hat{\mathbf{f}}$  and  $\hat{\sigma}$ . Using the 2D decorrelated squared  $W_2$  loss function also gives inaccurate  $\hat{\sigma}$ . Thus, the sliced  $W_2$  distance and the 2D decorrelated squared  $W_2$  loss are not good candidates for reconstructing multivariate SDEs. Numerically estimating Eq. (17) yields poorer performance than numerically estimating Eq. (18) because numerically evaluating the  $W_2$  distance for higher-dimensional empirical distributions is generally less accurate.

From Fig. 4(c), we see that the runtime and memory needed to numerically evaluate the time-decoupled Eq. (18) using `ot.emd2` is smaller than those needed for the MMD method, but larger than those needed to numerically estimate Eq. (17). Yet, as shown in Fig. 4(d), minimizing Eq. (18) leads to the fastest convergence, potentially requiring fewer epochs when using Eq. (18) as the loss function. An additional comparison of using the two loss functions, the finite-time-point squared  $W_2$  distance Eq. (17) and the finite-time-point time-decoupled squared  $W_2$  distance Eq. (18) is given in Appendix J. Further analysis on how the number of samples and the dimensionality of an SDE dimensionality affects  $W_2$ -based distances in reconstructing multivariate SDEs will be informative.

## 6 Summary and Conclusions

In this paper, we analyzed the squared  $W_2$  distance between two probability distributions associated with two SDEs and proposed a novel method for efficient reconstruction of SDEs from data by minimizing squared  $W_2$  distances as loss functions. Upon performing numerical experiments, we found that our proposed finite-time-point time-decoupled squared  $W_2$  distance loss function, Eq. (18), is superior than many other recently developed machine-learning and statistical approaches to SDE reconstruction.

A number of extensions are apparent. First, one can further investigate applying the squared  $W_2$  loss to the reconstruction of high-dimensional SDEs. Another important direction to develop are approaches to efficiently evaluate the squared  $W_2$  loss function Eq. (17) and analyze how well the time-decoupled squared  $W_2$  loss function Eq. (18) can approximate Eq. (17). Whether the Wasserstein distance can serve as upper bounds for the errors  $f - \hat{f}$  and  $\sigma - \hat{\sigma}$  is also an intriguing question as its resolution will determine if minimizing the squared Wasserstein distance is sufficient for reconstructing SDEs. Finally, another promising area worthy of study is the extension of the squared  $W_2$  distance loss function to the reconstruction of general Lévy processes that include jumps in the trajectories.

## Acknowledgments and Disclosure of Funding

The authors acknowledge Dr. Hedi Xia for his constructive comments on this manuscript. TC acknowledges support from the Army Research Office through grant W911NF-18-1-0345.

## References

- Martin Arjovsky, Soumith Chintala, and Léon Bottou. Wasserstein generative adversarial networks. In *International Conference on Machine Learning*, pages 214–223. PMLR, 2017.
- Daniel Bartl, Mathias Beiglböck, and Gudmund Pammer. The Wasserstein space of stochastic processes. *arXiv preprint arXiv:2104.14245*, 2021.
- Jocelyne Bion-Nadal and Denis Talay. On a Wasserstein-type distance between solutions to stochastic differential equations. *The Annals of Applied Probability*, 29(3):1609–1639, 2019. doi: 10.1214/18-aap1423.
- Paul C Bressloff. *Stochastic Processes in Cell Biology*, volume 41. Springer, 2014.
- Francois-Xavier Briol, Alessandro Barp, Andrew B Duncan, and Mark Girolami. Statistical inference for generative models with maximum mean discrepancy. *arXiv preprint arXiv:1906.05944*, 2019.
- Ricky TQ Chen, Yulia Rubanova, Jesse Bettencourt, and David K Duvenaud. Neural ordinary differential equations. In *Advances in Neural Information Processing Systems*, volume 31, 2018.
- Sinho Chewi, Julien Clancy, Thibaut Le Gouic, Philippe Rigollet, George Stepaniants, and Austin Stromme. Fast and smooth interpolation on Wasserstein space. In *International Conference on Artificial Intelligence and Statistics*, pages 3061–3069. PMLR, 2021.
- Erhan Cinlar. *Probability and Stochastics*. Springer Science & Business Media, 2011.
- Philippe Clement and Wolfgang Desch. An elementary proof of the triangle inequality for the Wasserstein metric. *Proceedings of the American Mathematical Society*, 136(1): 333–339, 2008.
- Marco Cuturi, Olivier Teboul, and Jean-Philippe Vert. Differentiable ranks and sorting using optimal transport. In *Proceedings of the 33rd International Conference on Neural Information Processing Systems*, pages 6861–6871, 2019.

- Francesco C De Vecchi, Paola Morando, and Stefania Ugolini. Reduction and reconstruction of stochastic differential equations via symmetries. *Journal of Mathematical Physics*, 57(12), 2016.
- Rémi Flamary, Nicolas Courty, Alexandre Gramfort, Mokhtar Z Alaya, Aurélie Boisbunon, Stanislas Chambon, Laetitia Chapel, Adrien Corenflos, Kilian Fatras, Nemo Fournier, et al. Pot: Python optimal transport. *The Journal of Machine Learning Research*, 22(1):3571–3578, 2021.
- Nicolas Fournier and Arnaud Guillin. On the rate of convergence in Wasserstein distance of the empirical measure. *Probability Theory and Related Fields*, 162(3-4):707–738, 2015.
- Charlie Frogner, Chiyuan Zhang, Hossein Mobahi, Mauricio Araya, and Tomaso A Poggio. Learning with a Wasserstein loss. In *Advances in Neural Information Processing Systems*, volume 28, 2015.
- Kaiming He, Xiangyu Zhang, Shaoqing Ren, and Jian Sun. Deep residual learning for image recognition. In *Proceedings of the IEEE conference on computer vision and pattern recognition*, pages 770–778, 2016.
- Junteng Jia and Austin R Benson. Neural jump stochastic differential equations. *Advances in Neural Information Processing Systems*, 32, 2019.
- Patrick Kidger, James Foster, Xuechen Li, and Terry J Lyons. Neural SDEs as infinite-dimensional GANs. In *International Conference on Machine Learning*, pages 5453–5463. PMLR, 2021.
- Soheil Kolouri, Gustavo K Rohde, and Heiko Hoffmann. Sliced Wasserstein distance for learning Gaussian mixture models. In *Proceedings of the IEEE Conference on Computer Vision and Pattern Recognition*, pages 3427–3436, 2018.
- Soheil Kolouri, Kimia Nadjahi, Umut Simsekli, Roland Badeau, and Gustavo Rohde. Generalized sliced Wasserstein distances. In *Advances in Neural Information Processing Systems*, volume 32, 2019.
- Xuechen Li, Ting-Kam Leonard Wong, Ricky TQ Chen, and David Duvenaud. Scalable gradients for stochastic differential equations. In *International Conference on Artificial Intelligence and Statistics*, pages 3870–3882. PMLR, 2020.
- Yujia Li, Kevin Swersky, and Rich Zemel. Generative moment matching networks. In *International Conference on Machine Learning*, pages 1718–1727. PMLR, 2015.
- Yen Ting Lin and Nicolas E Buchler. Efficient analysis of stochastic gene dynamics in the non-adiabatic regime using piecewise deterministic Markov processes. *Journal of The Royal Society Interface*, 15(138):20170804, 2018.

- Haitao Liu, Yew-Soon Ong, Xiaobo Shen, and Jianfei Cai. When Gaussian process meets big data: a review of scalable GPs. *IEEE Transactions on Neural Networks and Learning Systems*, 31(11):4405–4423, 2020.
- David JC MacKay et al. Introduction to Gaussian processes. *NATO ASI Series F Computer and Systems Sciences*, 168:133–166, 1998.
- Lionel Mathelin, M Yousuff Hussaini, and Thomas A Zang. Stochastic approaches to uncertainty quantification in CFD simulations. *Numerical Algorithms*, 38:209–236, 2005.
- Marek Musiela and Marek Rutkowski. *Martingale Methods in Financial Modelling*, volume 36. Springer Science & Business Media, 2006.
- Jung Hun Oh, Maryam Pouryahya, Aditi Iyer, Aditya P Apte, Allen Tannenbaum, and Joseph O Deasy. Kernel Wasserstein distance. *arXiv preprint arXiv:1905.09314*, 2019.
- José Pereira, Morteza Ibrahimi, and Andrea Montanari. Learning networks of stochastic differential equations. In *Advances in Neural Information Processing Systems*, volume 23, 2010.
- Mark Rowland, Jiri Hron, Yunhao Tang, Krzysztof Choromanski, Tamas Sarlos, and Adrian Weller. Orthogonal estimation of Wasserstein distances. In *The 22nd International Conference on Artificial Intelligence and Statistics*, pages 186–195. PMLR, 2019.
- Ludger Rüschendorf. The Wasserstein distance and approximation theorems. *Probability Theory and Related Fields*, 70(1):117–129, 1985.
- Jesus Maria Sanz-Serna and Konstantinos C Zygalakis. Wasserstein distance estimates for the distributions of numerical approximations to ergodic stochastic differential equations. *The Journal of Machine Learning Research*, 22(1):11006–11042, 2021.
- Christian Soize. *Uncertainty Quantification*. Springer, 2017.
- Yang Song, Jascha Sohl-Dickstein, Diederik P Kingma, Abhishek Kumar, Stefano Ermon, and Ben Poole. Score-based generative modeling through stochastic differential equations. In *International Conference on Learning Representations*, 2020.
- Timothy John Sullivan. *Introduction to Uncertainty Quantification*, volume 63. Springer, 2015.
- Anh Tong, Thanh Nguyen-Tang, Toan Tran, and Jaesik Choi. Learning fractional white noises in neural stochastic differential equations. In *Advances in Neural Information Processing Systems*, volume 35, pages 37660–37675, 2022.
- Belinda Tzen and Maxim Raginsky. Neural stochastic differential equations: deep latent Gaussian models in the diffusion limit. *arXiv preprint arXiv:1905.09883*, 2019.

- Cédric Villani et al. *Optimal transport: old and new*, volume 338. Springer, 2009.
- Jian Wang.  $L^p$ -Wasserstein distance for stochastic differential equations driven by Lévy processes. *Bernoulli*, pages 1598–1616, 2016.
- Greg Welch, Gary Bishop, et al. An introduction to the Kalman filter. 1995.
- Gregory F Welch. Kalman filter. *Computer Vision: A Reference Guide*, pages 1–3, 2020.
- Wenbo Zheng, Fei-Yue Wang, and Chao Gou. Nonparametric different-feature selection using Wasserstein distance. In *2020 IEEE 32nd International Conference on Tools with Artificial Intelligence (ICTAI)*, pages 982–988. IEEE, 2020.

## Appendix A. Proof to Theorem 1

Here, we shall provide a proof to Theorem 1. First, note that  $\tilde{X}(t)$  defined in Eq. (10) is a specific realization of  $\hat{X}(t)$  defined in Eq. (2), *coupled to*  $X(t)$  in the sense that its initial values are  $X(0)$  almost surely and the Itô integral is defined with respect to the same standard Brownian motion  $B(t)$ . Therefore, by definition, if we let  $\pi$  in Eq. (4) to be the joint distribution of  $(X, \tilde{X})$ , then

$$W_2(\mu, \hat{\mu}) \leq \left( \mathbb{E} \left[ \int_0^T |\tilde{X}(t) - X(t)|^2 dt \right] \right)^{1/2}. \quad (35)$$

Next, we provide a bound for  $\mathbb{E} \left[ \int_0^T |\tilde{X}(t) - X(t)|^2 dt \right]^{\frac{1}{2}}$  by the mean value theorem for  $f$  and  $g$ .

$$\begin{aligned} d(X(t) - \tilde{X}(t)) &= \partial_x f(\eta_1(X(t), \tilde{X}(t), t), t) \cdot (X(t) - \tilde{X}(t)) dt \\ &\quad + \partial_x \sigma(\eta_2(X(t), \tilde{X}(t), t), t) \cdot (X(t) - \tilde{X}(t)) dB(t) \\ &\quad + (f - \hat{f})(\tilde{X}(t), t) dt + (\sigma - \hat{\sigma})(\tilde{X}(t), t) dB(t). \end{aligned} \quad (36)$$

where  $\eta_1(x_1, x_2), \eta_2(x_1, x_2)$  are defined in Eq. (8) such that their values are in  $(x_1, x_2)$ .

Applying Itô's formula to  $[X(t) - \tilde{X}(t)]/H(0; t)$ , we find

$$\begin{aligned} d \left( \frac{X(t) - \tilde{X}(t)}{H(0; t)} \right) &= \frac{1}{H(0; t)} \left[ (f - \hat{f})(\tilde{X}(t), t) dt + \partial_x \sigma(\eta_2(X, \tilde{X}), t) \cdot (\sigma - \hat{\sigma})(\tilde{X}(t), t) dt \right] \\ &\quad + \frac{1}{H(0; t)} \left[ (\sigma - \hat{\sigma})(\tilde{X}(t), t) dB(t) \right]. \end{aligned} \quad (37)$$

Integrating both sides from 0 to  $t$ , we obtain

$$\begin{aligned} X(t) - \tilde{X}(t) &= \int_0^t H(s; t) \left[ (f - \hat{f})(\tilde{X}(s), s) + \partial_x \sigma(\eta_2(X, \tilde{X}), s) \cdot (\sigma - \hat{\sigma})(\tilde{X}(s), s) \right] ds \\ &\quad + \int_0^t H(s; t) \cdot (\sigma - \hat{\sigma})(\tilde{X}(s), s) dB(s). \end{aligned} \quad (38)$$

By invoking Itô isometry and observing that  $(a + b + c)^2 \leq 3(a^2 + b^2 + c^2)$ , we deduce

$$\begin{aligned}
 \mathbb{E}[(X(t) - \tilde{X}(t))^2] &\leq 3\mathbb{E}\left[\left(\int_0^t H(s;t) \cdot (f - \hat{f})(\tilde{X}(s), s) ds\right)^2\right] \\
 &\quad + 3\mathbb{E}\left[\left(\int_0^t H(s;t) \cdot (\partial_x \sigma(\eta_2(X, \tilde{X}), s) \cdot (\sigma - \hat{\sigma})(\tilde{X}(s), s)) ds\right)^2\right] \\
 &\quad + 3\mathbb{E}\left[\left(\int_0^t H(s;t) \cdot (\sigma - \hat{\sigma})(\tilde{X}(s), s) dB(s)\right)^2\right] \\
 &\leq 3\mathbb{E}\left[\int_0^t H^2(s;t) ds\right] \times \mathbb{E}\left[\int_0^T (f - \hat{f})^2(\tilde{X}(s), s) ds\right] \\
 &\quad + 3\mathbb{E}\left[\int_0^t H^2(s;t) ds\right] \times \mathbb{E}\left[\int_0^T \left(\partial_x \sigma(\eta_2(X, \tilde{X}), s) \cdot (\sigma - \hat{\sigma})(\tilde{X}(s), s)\right)^2 ds\right] \quad (39) \\
 &\quad + 3\mathbb{E}\left[\int_0^t H^2(s;t) \cdot (\sigma - \hat{\sigma})^2(\tilde{X}(s), s) ds\right] \\
 &\leq 3\mathbb{E}\left[\int_0^t H^2(s;t) ds\right] \times \mathbb{E}\left[\int_0^t (f - \hat{f})^2(\tilde{X}(s), s) ds\right] \\
 &\quad + 3\mathbb{E}\left[\int_0^t H^2(s;t) ds\right] \times \mathbb{E}\left[\int_0^t \left(\partial_x \sigma(\eta_2(X, \tilde{X}), s) \cdot (\sigma - \hat{\sigma})(\tilde{X}(s), s)\right)^2 ds\right] \\
 &\quad + 3\left(\mathbb{E}\left[\int_0^t H^4(s;t) ds\right]\right)^{1/2} \times \left(\mathbb{E}\left[\int_0^t (\sigma - \hat{\sigma})^4(\tilde{X}(s), s) ds\right]\right)^{1/2}.
 \end{aligned}$$

Finally, we conclude that

$$\begin{aligned}
 W_2^2(\mu, \tilde{\mu}) &\leq \int_0^T \mathbb{E}[(X(t) - \tilde{X}(t))^2] dt \\
 &\leq 3 \int_0^T \mathbb{E}\left[\int_0^t H^2(s;t) ds\right] dt \times \mathbb{E}\left[\int_0^T (f - \hat{f})^2(\tilde{X}(s), s) ds\right] \\
 &\quad + 3 \int_0^T \mathbb{E}\left[\int_0^t H^2(s;t) ds\right] dt \times \mathbb{E}\left[\int_0^T \left(\partial_x \sigma(\eta_2(X, \tilde{X}), s) \cdot (\sigma - \hat{\sigma})(\tilde{X}(s), s)\right)^2 ds\right] \\
 &\quad + 3 \int_0^T \left(\mathbb{E}\left[\int_0^t H^4(s;t) ds\right]\right)^{1/2} dt \times \left(\mathbb{E}\left[\int_0^T (\sigma - \hat{\sigma})^4(\tilde{X}(s), s) ds\right]\right)^{1/2}, \quad (40)
 \end{aligned}$$

which proves Theorem 1.

This theorem can be generalized to higher dimensional dynamics of  $\mathbf{X}(t)$  and  $\hat{\mathbf{X}}(t)$  described by

$$\begin{aligned}
 d\mathbf{X}(t) &= \mathbf{f}(\mathbf{X}(t), t) dt + \boldsymbol{\sigma}(\mathbf{X}(t), t) d\mathbf{B}(t), \\
 d\hat{\mathbf{X}}(t) &= \hat{\mathbf{f}}(\hat{\mathbf{X}}(t), t) dt + \hat{\boldsymbol{\sigma}}(\hat{\mathbf{X}}(t), t) d\hat{\mathbf{B}}(t), \quad (41)
 \end{aligned}$$

where  $\mathbf{f}, \hat{\mathbf{f}} : \mathbb{R}^{d+1} \rightarrow \mathbb{R}^d$  are the  $d$ -dimensional drift functions and  $\boldsymbol{\sigma}, \hat{\boldsymbol{\sigma}} : \mathbb{R}^{d+1} \rightarrow \mathbb{R}^{d \times s}$  are diffusion matrices.  $\mathbf{B}(t)$  and  $\hat{\mathbf{B}}(t)$  are two independent  $s$ -dimensional standard Brownian motions. Under some additional assumptions, one can derive an upper bound for the  $W_2$  distance of the probability distributions for  $\mathbf{X}, \hat{\mathbf{X}}$  as in Eq. (9). For example, if

for every  $i = 1, \dots, d$ , the  $i^{\text{th}}$  component  $dX_i(t) = f_i(X_i(t), t)dt + \sigma_i(X_i(t), t)dB_i(t)$  and  $d\hat{X}_i(t) = \hat{f}_i(\hat{X}_i(t), t)dt + \hat{\sigma}_i(\hat{X}_i(t), t)d\hat{B}_i(t)$ , where  $B_i(t), \hat{B}_i(t)$  are independent Brownian motions, then similar conclusions can be derived by calculating the difference  $X_i - \hat{X}_i$ . Developing an upper bound of the  $W_2$  distance for general dimensions  $d$  requires additional assumptions to find expressions for  $\mathbf{X} - \hat{\mathbf{X}}$ . We leave this nontrivial derivation as future work. Although without a formal theoretical analysis, we shall show in Example 4 that applying the squared  $W_2$  distance as the loss function is also effective in reconstructing multidimensional SDEs.

## Appendix B. Single-trajectory MSE and KL divergence

We shall first show that using the single-trajectory MSE tends to fit the mean process  $\mathbb{E}[X(t)]$  and make noise diminish, which indicates that the MSE is not a good loss function when one wishes to fit  $\sigma$  in Eq. (1).

For two *independent*  $d$ -dimensional stochastic processes  $\{\mathbf{X}(t)\}_{t=0}^T, \{\hat{\mathbf{X}}(t)\}_{t=0}^T$  as solutions to Eq. (41) with appropriate  $\mathbf{f}, \hat{\mathbf{f}}$  and  $\boldsymbol{\sigma}, \hat{\boldsymbol{\sigma}}$ , let  $\mathbb{E}[\mathbf{X}]$  represent the trajectory of mean values of  $\mathbf{X}(t)$ , *i.e.*,  $\mathbb{E}[\mathbf{X}] = \mathbb{E}[\mathbf{X}(t)]$ . We have

$$\begin{aligned} \mathbb{E}[\|\mathbf{X} - \hat{\mathbf{X}}\|^2] &= \mathbb{E}[\|\mathbf{X} - \mathbb{E}[\mathbf{X}]\|^2] + \mathbb{E}[\|\hat{\mathbf{X}} - \mathbb{E}[\mathbf{X}]\|^2] \\ &\quad - 2\mathbb{E}\left[\int_0^T (\mathbf{X} - \mathbb{E}[\mathbf{X}], \hat{\mathbf{X}} - \mathbb{E}[\mathbf{X}]) dt\right], \end{aligned} \quad (42)$$

where  $\|\mathbf{X}\|^2 := \int_0^T \|\mathbf{X}\|_2^2 dt$ ,  $\|\cdot\|_2$  denotes the  $\ell^2$  norm of a vector, and  $(\cdot, \cdot)$  is the inner product of two  $d$ -dimensional vectors. In view of the independence between  $\mathbf{X} - \mathbb{E}[\mathbf{X}]$  and  $\hat{\mathbf{X}} - \mathbb{E}[\mathbf{X}]$ , we have  $\mathbb{E}[(\mathbf{X} - \mathbb{E}[\mathbf{X}], \hat{\mathbf{X}} - \mathbb{E}[\mathbf{X}])] = \mathbb{E}[(\mathbf{X} - \mathbb{E}[\mathbf{X}])] \cdot \mathbb{E}[(\hat{\mathbf{X}} - \mathbb{E}[\mathbf{X}])] = 0$ , and

$$\mathbb{E}[\|\mathbf{X} - \hat{\mathbf{X}}\|^2] \geq \mathbb{E}[\|\mathbf{X} - \mathbb{E}[\mathbf{X}]\|^2]. \quad (43)$$

Therefore, the optimal  $\hat{\mathbf{X}}$  that minimizes the MSE is  $\hat{\mathbf{X}} = \mathbb{E}[\mathbf{X}]$ , which indicates that the MSE tends to fit the mean process  $\mathbb{E}[\mathbf{X}]$  and make noise diminish. This is not desirable when one wishes to fit a nonzero  $\sigma$  in Eq. (1).

The KL divergence, in some cases, will diverge and thus is not suitable for being used as a loss function. Here, we provide a simple intuitive example when the KL divergence fail. If we consider the degenerate case when  $dX(t) = dt, d\hat{X}(t) = (1 - \epsilon)dt, t \in [0, T]$ , then  $D_{KL}(\mu, \hat{\mu}) = \infty$  no matter how small  $\epsilon \neq 0$  is because  $\mu, \hat{\mu}$  has different and degenerate support. However, from Theorem 1,  $\lim_{\epsilon \rightarrow 0} W_2(\mu, \hat{\mu}) = 0$ . Therefore, the KL divergence cannot effectively measure the similarity between  $\mu, \hat{\mu}$ . Overall, the squared  $W_2$  distance is a better metric than some of the commonly used loss metrics such as the MSE or the KL divergence.

### Appendix C. Proof to Theorem 2

Here, we shall prove Theorem 2. We denote

$$\Omega_N := \{\mathbf{Y}(t) | \mathbf{Y}(t) = \mathbf{Y}(t_i) \ t \in [t_i, t_{i+1}), i < N - 1; \ \mathbf{Y}(t) = \mathbf{Y}(t_i), \ t \in [t_i, t_{i+1}]\} \quad (44)$$

to be the space of piecewise functions. We also define the space

$$\tilde{\Omega}_N := \{\mathbf{Y}_1(t) + \mathbf{Y}_2(t), \mathbf{Y}_1 \in C([0, T]; \mathbb{R}^d), \mathbf{Y}_2 \in \Omega_N\}. \quad (45)$$

$\tilde{\Omega}_N$  is also a separable metric space because both  $(C([0, T]; \mathbb{R}^d), \|\cdot\|)$  and  $(\Omega_N, \|\cdot\|)$  are separable metric spaces. Furthermore, both the embedding mapping from  $C([0, T]; \mathbb{R}^d)$  to  $\tilde{\Omega}_N$  and the embedding mapping from  $\Omega_N$  to  $\tilde{\Omega}_N$  preserves the  $\|\cdot\|$  norm. Then, the two embedding mappings are measurable, which enables us to define the measures on  $\mathcal{B}(\tilde{\Omega}_N)$  induced by the measures  $\mu, \hat{\mu}$  on  $\mathcal{B}(C([0, T]; \mathbb{R}^d))$  and the measures  $\mu_N, \hat{\mu}_N$  on  $\mathcal{B}(\Omega_N)$ . For notational simplicity, we shall still denote those induced measures by  $\mu, \hat{\mu}, \mu_N, \hat{\mu}_N$ .

Therefore, the inequality Eq. (14) is a direct result of the triangular inequality for the Wasserstein distance (Clement and Desch, 2008) because  $\mathbf{X}, \mathbf{X}_N, \hat{\mathbf{X}}, \hat{\mathbf{X}}_N \in \tilde{\Omega}_N$ .

Next, we shall prove Eq. (16) when  $\mathbf{X}(t), \hat{\mathbf{X}}(t)$  are solutions to SDEs Eq. (1) and Eq. (2). Because  $\mathbf{X}_N(t)$  is the projection to  $\mathbf{X}(t)$ , the squared  $W_2^2(\mu, \mu_N)$  can be bounded by

$$W_2^2(\mu, \mu_N) \leq \sum_{i=1}^N \int_{t_{i-1}}^{t_i} \mathbb{E}[|\mathbf{X}(t) - \mathbf{X}_N(t)|_2^2] dt = \sum_{i=1}^N \int_{t_{i-1}}^{t_i} \sum_{\ell=1}^d \mathbb{E}[(X_\ell(t) - X_{N,\ell}(t))^2] dt \quad (46)$$

For the first inequality above, we choose a specific *coupling*, i.e. the coupled distribution,  $\pi$  of  $\mu, \mu_N$  that is essentially the ‘‘original’’ probability distribution. To be more specific, for an abstract probability space  $(\Omega, \mathcal{A}, p)$  associated with  $\mathbf{X}, \mu$  and  $\mu_N$  can be characterized by the *pushforward* of  $p$  via  $\mathbf{X}$  and  $\mathbf{X}_N$  respectively, i.e.,  $\mu = \mathbf{X}_*p$ , defined by  $\forall A \in \mathcal{B}(\tilde{\Omega}_N)$ , elements in the Borel  $\sigma$ -algebra of  $\tilde{\Omega}_N$ ,

$$\mu(A) = \mathbf{X}_*p(A) := p(\mathbf{X}^{-1}(A)), \quad (47)$$

where  $\mathbf{X}$  is interpreted as a measurable map from  $\Omega$  to  $\tilde{\Omega}_N$ , and  $\mathbf{X}^{-1}(A)$  is the preimage of  $A$  under  $\mathbf{X}$ . Then, the coupling  $\pi$  is defined by

$$\pi = (\mathbf{X}, \mathbf{X}_N)_*p, \quad (48)$$

where  $(\mathbf{X}, \mathbf{X}_N)$  is interpreted as a measurable map from  $\Omega$  to  $\tilde{\Omega}_N \times \tilde{\Omega}_N$ . One can readily verify that the marginal distributions of  $\pi$  are  $\mu$  and  $\mu_N$  respectively. Recall that  $s$  represents the dimension of the standard Brownian motions in the SDEs.

For each  $\ell = 1, \dots, d$ , we have

$$\begin{aligned}
 & \sum_{i=1}^N \int_{t_{i-1}}^{t_i} \mathbb{E}[(X_\ell(t) - X_{N,\ell}(t))^2] dt \\
 & \leq (s+1) \left[ \sum_{i=1}^N \int_{t_{i-1}}^{t_i} \left( \mathbb{E} \left[ \left( \int_{t_i}^t f_\ell(\hat{X}(r), r) dr \right)^2 \right] + \mathbb{E} \left[ \left( \int_{t_i}^t \sum_{j=1}^s \sigma_{\ell,j}(\hat{X}(r), r) dB_j(r) \right)^2 \right] \right) dt \right] \\
 & \leq (s+1) \sum_{i=1}^N \left( (\Delta t)^2 \mathbb{E} \left[ \int_{t_{i-1}}^{t_i} f_\ell^2 dt \right] + \Delta t \sum_j \mathbb{E} \left[ \int_{t_{i-1}}^{t_i} \sigma_{\ell,j}^2 dt \right] \right)
 \end{aligned} \tag{49}$$

The first inequality follows from the observation that  $(\sum_{i=1}^n a_i)^2 \leq n(\sum_{i=1}^n a_i^2)$  and application of this observation to the integral representation of  $\mathbf{X}(t)$ . Summing over  $\ell$ , we have

$$\left( \sum_{i=1}^N \int_{t_{i-1}}^{t_i} \mathbb{E}[\|\mathbf{X}(t) - \mathbf{X}_N(t)\|_2^2] dt \right)^{1/2} \leq \sqrt{s+1} \left( F(\Delta t)^2 + \Sigma \Delta t \right)^{1/2} \tag{50}$$

Similarly,  $W_2(\hat{\mu}, \hat{\mu}_N)$  can be bounded by

$$W_2(\hat{\mu}, \hat{\mu}_N) \leq \sqrt{s+1} \sqrt{\hat{F}(\Delta t)^2 + \hat{\Sigma} \Delta t}. \tag{51}$$

Substituting Eq. (50) and Eq. (51) into Eq. (14), we have proved Eq. (16). This completes the proof of Theorem 2.

### Appendix D. Proof to Theorem 3

We now give a proof to Theorem 3. First, we notice that

$$\mathbb{E} \left[ \|\mathbf{X}(t) - \hat{\mathbf{X}}(t)\|_2^2 \right] \leq 2(FT + \hat{F}T + \Sigma + \hat{\Sigma}) < \infty, \quad \forall t \in [0, T] \tag{52}$$

where  $F, \hat{F}, \Sigma, \hat{\Sigma}$  are defined in Eq. (15). We denote

$$M := \max_{t \in [0, T]} W_2(\mu(t), \hat{\mu}(t)) \leq 2(FT + \hat{F}T + \Sigma + \hat{\Sigma}). \tag{53}$$

By applying Theorem 2 with  $N = 1$ , the bound

$$\begin{aligned}
 & \inf_{\pi_i} \sqrt{\mathbb{E}_{\pi_i} [\|\mathbf{X}(t_i) - \hat{\mathbf{X}}(t_i)\|_2^2] \Delta t - \sqrt{(s+1)\Delta t} \left( \sqrt{F_i \Delta t + \Sigma_i} + \sqrt{\hat{F}_i \Delta t + \hat{\Sigma}_i} \right)} \leq W_2(\mu_i, \hat{\mu}_i) \\
 & \leq \inf_{\pi_i} \sqrt{\mathbb{E}_{\pi_i} [\|\mathbf{X}(t_i) - \hat{\mathbf{X}}(t_i)\|_2^2] \Delta t + \sqrt{(s+1)\Delta t} \left( \sqrt{F_i \Delta t + \Sigma_i} + \sqrt{\hat{F}_i \Delta t + \hat{\Sigma}_i} \right)}.
 \end{aligned} \tag{54}$$

holds true for all  $i = 1, 2, \dots, N-1$ . In Eq. (54),

$$\begin{aligned}
 F_i &:= \mathbb{E} \left[ \int_{t_i}^{t_{i+1}} \sum_{\ell=1}^d f_{\ell}^2(\mathbf{X}(t), t) dt \right] < \infty, \quad \Sigma_i := \mathbb{E} \left[ \int_{t_i}^{t_{i+1}} \sum_{\ell=1}^d \sum_{j=1}^s \sigma_{\ell,j}^2(\mathbf{X}(t), t) dt \right] < \infty, \\
 \hat{F}_i &:= \mathbb{E} \left[ \int_{t_i}^{t_{i+1}} \sum_{\ell=1}^d \hat{f}_{\ell}^2(\hat{\mathbf{X}}(t), t) dt \right] < \infty, \quad \hat{\Sigma}_i := \mathbb{E} \left[ \int_{t_i}^{t_{i+1}} \sum_{\ell=1}^d \sum_{j=1}^s \hat{\sigma}_{\ell,j}^2(\hat{\mathbf{X}}(t), t) dt \right] < \infty,
 \end{aligned} \tag{55}$$

which results from

$$\sum_{i=0}^{N-1} F_i = F < \infty, \quad \sum_{i=0}^{N-1} \hat{F}_i = \hat{F} < \infty, \quad \sum_{i=0}^{N-1} \Sigma_i = \Sigma < \infty, \quad \sum_{i=0}^{N-1} \hat{\Sigma}_i = \hat{\Sigma} < \infty, \tag{56}$$

where  $F, \hat{F}, \Sigma, \hat{\Sigma}$  are defined in Eq. (15). Squaring the inequality (54), we have

$$\begin{aligned}
 W_2^2(\boldsymbol{\mu}_i, \hat{\boldsymbol{\mu}}_i) &\leq \inf_{\pi_i} \mathbb{E}_{\pi_i} [|\mathbf{X}(t_i) - \hat{\mathbf{X}}(t_i)|_2^2] \Delta t \\
 &\quad + 2 \inf_{\pi_i} \sqrt{\mathbb{E}_{\pi_i} [|\mathbf{X}(t_i) - \hat{\mathbf{X}}(t_i)|_2^2]} \sqrt{(s+1)\Delta t} \left( \sqrt{F_i \Delta t + \Sigma_i} + \sqrt{\hat{F}_i \Delta t + \hat{\Sigma}_i} \right) \\
 &\quad + 2(s+1)\Delta t (F_i \Delta t + \Sigma_i + \hat{F}_i \Delta t + \hat{\Sigma}_i), \\
 W_2^2(\boldsymbol{\mu}_i, \hat{\boldsymbol{\mu}}_i) &\geq \inf_{\pi_i} \mathbb{E}_{\pi_i} [|\mathbf{X}(t_i) - \hat{\mathbf{X}}(t_i)|_2^2] \Delta t \\
 &\quad - 2W_2(\boldsymbol{\mu}_i, \hat{\boldsymbol{\mu}}_i) \sqrt{(s+1)\Delta t} \left( \sqrt{F_i \Delta t + \Sigma_i} + \sqrt{\hat{F}_i \Delta t + \hat{\Sigma}_i} \right) \\
 &\quad - 2(s+1)\Delta t (F_i \Delta t + \Sigma_i + \hat{F}_i \Delta t + \hat{\Sigma}_i)
 \end{aligned} \tag{57}$$

Specifically, from Eq. (53) and Eq. (54),

$$W_2(\boldsymbol{\mu}_i, \hat{\boldsymbol{\mu}}_i) \leq \sqrt{\Delta t} \left[ M + \sqrt{s+1} \left( \sqrt{FT + \Sigma} + \sqrt{\hat{F}T + \hat{\Sigma}} \right) \right] := \tilde{M} \sqrt{\Delta t}, \quad \tilde{M} < \infty \tag{58}$$

Summing over  $i = 1, \dots, N-1$  for both inequalities in Eq. (57) and noting that  $\Delta t = \frac{T}{N}$ , we conclude

$$\begin{aligned}
 \sum_{i=1}^{N-1} W_2^2(\boldsymbol{\mu}_i, \hat{\boldsymbol{\mu}}_i) &\leq \sum_{i=1}^{N-1} \inf_{\pi_i} \mathbb{E}_{\pi_i} \left[ |\mathbf{X}(t_i) - \hat{\mathbf{X}}(t_i)|_2^2 \right] \Delta t \\
 &\quad + 2M\Delta t\sqrt{s+1} \sum_{i=1}^{N-1} \left( \sqrt{F_i\Delta t + \Sigma_i} + \sqrt{\hat{F}_i\Delta t + \hat{\Sigma}_i} \right) \\
 &\quad + 2\Delta t(s+1)(F\Delta t + \Sigma + \hat{F}\Delta t + \hat{\Sigma}), \\
 &\leq \sum_{i=1}^{N-1} \inf_{\pi_i} \mathbb{E}_{\pi_i} \left[ |\mathbf{X}(t_i) - \hat{\mathbf{X}}(t_i)|_2^2 \right] \Delta t \\
 &\quad + 2(s+1)\Delta t(F\Delta t + \Sigma + \hat{F}\Delta t + \hat{\Sigma}) \\
 &\quad + M\sqrt{(s+1)\Delta t} ((F + \hat{F} + 2T)\sqrt{\Delta t} + \Sigma + \hat{\Sigma} + 2T)
 \end{aligned} \tag{59}$$

and

$$\begin{aligned}
 \sum_{i=1}^{N-1} W_2^2(\boldsymbol{\mu}_i, \hat{\boldsymbol{\mu}}_i) &\geq \sum_{i=1}^{N-1} \inf_{\pi_i} \mathbb{E}_{\pi_i} \left[ |\mathbf{X}(t_i) - \hat{\mathbf{X}}(t_i)|_2^2 \right] \Delta t \\
 &\quad - 2\tilde{M}\Delta t\sqrt{s+1} \sum_{i=1}^{N-1} \left( \sqrt{F_i\Delta t + \Sigma_i} + \sqrt{\hat{F}_i\Delta t + \hat{\Sigma}_i} \right) \\
 &\quad - 2(s+1)\Delta t(F\Delta t + \Sigma + \hat{F}\Delta t + \hat{\Sigma}), \\
 &\geq \sum_{i=1}^{N-1} \inf_{\pi_i} \mathbb{E}_{\pi_i} \left[ |\mathbf{X}(t_i) - \hat{\mathbf{X}}(t_i)|_2^2 \right] \Delta t \\
 &\quad - 2(s+1)\Delta t(F\Delta t + \Sigma + \hat{F}\Delta t + \hat{\Sigma}) \\
 &\quad - \tilde{M}\sqrt{(s+1)\Delta t} ((F + \hat{F} + 2T)\sqrt{\Delta t} + \Sigma + \hat{\Sigma} + 2T).
 \end{aligned} \tag{60}$$

Eqs. (59) and (60) indicate that as  $N \rightarrow \infty$ ,

$$\sum_{i=1}^{N-1} \inf_{\pi_i} \mathbb{E}_{\pi_i} \left[ |\mathbf{X}(t_i) - \hat{\mathbf{X}}(t_i)|_2^2 \right] \Delta t - \sum_{i=1}^{N-1} W_2^2(\boldsymbol{\mu}_i, \hat{\boldsymbol{\mu}}_i) \rightarrow 0, \tag{61}$$

Suppose  $0 = t_0^1 < t_1^1 < \dots < t_{N_1}^1 = T$ ;  $0 = t_0^2 < t_1^2 < \dots < t_{N_2}^2 = T$  to be two sets of grids on  $[0, T]$ . We define a third set of grids  $0 = t_0^3 < \dots < t_{N_3}^3 = T$  such that  $\{t_0^1, \dots, t_{N_1}^1\} \cup \{t_0^2, \dots, t_{N_2}^2\} = \{t_0^3, \dots, t_{N_3}^3\}$ . Let  $\delta t := \max\{\max_i(t_{i+1}^1 - t_i^1), \max_j(t_{j+1}^2 - t_j^2), \max_k(t_{k+1}^3 - t_k^3)\}$ . We denote  $\mu(t_i^1)$  and  $\hat{\mu}(t_i^1)$  to be the probability distribution of  $\mathbf{X}(t_i^s)$  and  $\hat{\mathbf{X}}(t_i^s)$ ,  $s = 1, 2, 3$ , respectively. We will prove

$$\left| \sum_{i=0}^{N_1-1} W_2^2(\mu(t_i^1), \hat{\mu}(t_i^1))(t_{i+1}^1 - t_i^1) - \sum_{i=0}^{N_3-1} W_2^2(\mu(t_i^3), \hat{\mu}(t_i^3))(t_{i+1}^3 - t_i^3) \right| \rightarrow 0, \tag{62}$$

as  $\delta t \rightarrow 0$ .

First, suppose in the interval  $(t_i^1, t_{i+1}^1)$ , we have  $t_i^1 = t_\ell^3 < t_{\ell+1} < \dots < t_{\ell+s}^3 = t_{i+1}^1, s \geq 1$ , then for  $s > 1$ , since  $t_{i+1}^1 - t_i^1 = \sum_{k=\ell}^{\ell+s-1} (t_{k+1}^3 - t_k^3)$ , we have

$$\begin{aligned} & \left| W_2^2(\mu(t_i^1), \hat{\mu}(t_i^1))(t_{i+1}^1 - t_i^1) - \sum_{k=\ell}^{\ell+s-1} W_2^2(\mu(t_k^3), \hat{\mu}(t_k^3))(t_{k+1}^3 - t_k^3) \right| \\ & \leq \sum_{k=\ell+1}^{\ell+s-1} \left| W_2(\mu(t_i^1), \hat{\mu}(t_i^1)) - W_2(\mu(t_k^3), \hat{\mu}(t_k^3)) \right| \\ & \quad \times \left( W_2(\mu(t_i^1), \hat{\mu}(t_i^1)) + W_2(\mu(t_k^3), \hat{\mu}(t_k^3)) \right) (t_{k+1}^3 - t_k^3). \end{aligned} \quad (63)$$

On the other hand, because we can take a specific coupling  $\pi^*$  to be the joint distribution of  $(\mathbf{X}(t_i^1), \mathbf{X}(t_k^3))$ ,

$$\begin{aligned} W_2(\mu(t_i^1), \mu(t_k^3)) & \leq \left( \mathbb{E}[|\mathbf{X}(t_k^3) - \mathbf{X}(t_i^1)|_2^2] \right)^{1/2} \\ & \leq \sqrt{s+1} \mathbb{E} \left[ \int_{t_i}^{t_{i+1}} \sum_{\ell=1}^d f_\ell^2(\mathbf{X}(t), t) dt + \sum_{\ell=1}^d \sum_{j=1}^s \sigma_{\ell,j}^2(\mathbf{X}(t), t) dt \right]^{1/2}. \end{aligned} \quad (64)$$

Similarly, we have

$$W_2(\hat{\mu}(t_i^1), \hat{\mu}(t_k^3)) \leq \sqrt{s+1} \mathbb{E} \left[ \int_{t_i}^{t_{i+1}} \sum_{\ell=1}^d \hat{f}_\ell^2(\mathbf{X}(t), t) dt + \sum_{\ell=1}^d \sum_{j=1}^s \hat{\sigma}_{\ell,j}^2(\mathbf{X}(t), t) dt \right]^{1/2} \quad (65)$$

From the triangular inequality of the Wasserstein distance, we find

$$\left| W_2(\mu(t_i^1), \hat{\mu}(t_i^1)) - W_2(\mu(t_k^3), \hat{\mu}(t_k^3)) \right| \leq W_2(\mu(t_i^1), \mu(t_k^3)) + W_2(\hat{\mu}(t_i^1), \hat{\mu}(t_k^3)). \quad (66)$$

Substituting Eq. (66) into Eq. (63), we conclude that

$$\begin{aligned} & \left| W_2^2(\mu(t_i^1), \hat{\mu}(t_i^1))(t_{i+1}^1 - t_i^1) - \sum_{k=\ell}^{\ell+s-1} W_2^2(\mu(t_k^3), \hat{\mu}(t_k^3))(t_{k+1}^3 - t_k^3) \right| \\ & \leq 2M(t_{i+1}^1 - t_i^1) \left( \sqrt{F_i \delta t + \Sigma_i} + \sqrt{\hat{F}_i \delta t + \hat{\Sigma}_i} \right). \end{aligned} \quad (67)$$

When the conditions in Eq. (22) hold true, we use Eq. (67) in Eq. (62) to find

$$\begin{aligned} & \left| \sum_{i=0}^{N_1-1} W_2^2(\mu(t_i^1), \hat{\mu}(t_i^1))(t_{i+1}^1 - t_i^1) - \sum_{i=0}^{N_3-1} W_2^2(\mu(t_i^3), \hat{\mu}(t_i^3))(t_{i+1}^3 - t_i^3) \right| \\ & \leq 2MT \max_i \left( \sqrt{F_i \delta t + \Sigma_i} + \sqrt{\hat{F}_i \delta t + \hat{\Sigma}_i} \right) \rightarrow 0 \end{aligned} \quad (68)$$

as  $\delta t \rightarrow 0$ . Similarly,

$$\begin{aligned} & \left| \sum_{i=0}^{N_2-1} W_2^2(\mu(t_i^2), \hat{\mu}(t_i^2))(t_{i+1}^2 - t_i^2) - \sum_{i=0}^{N_3-1} W_2^2(\mu(t_i^3), \hat{\mu}(t_i^3))(t_{i+1}^3 - t_i^3) \right| \\ & \leq 2MT \max_i \left( \sqrt{F_i \delta t + \Sigma_i} + \sqrt{\hat{F}_i \delta t + \hat{\Sigma}_i} \right) \rightarrow 0 \end{aligned} \quad (69)$$

as  $\delta t \rightarrow 0$ . Thus,

$$\left| \sum_{i=0}^{N_1-1} W_2^2(\mu(t_i^1), \hat{\mu}(t_i^1))(t_{i+1}^1 - t_i^1) - \sum_{i=0}^{N_2-1} W_2^2(\mu(t_i^2), \hat{\mu}(t_i^2))(t_{i+1}^2 - t_i^2) \right| \rightarrow 0 \quad (70)$$

as  $\delta t \rightarrow 0$ , which implies the limit

$$\lim_{N \rightarrow \infty} \sum_{i=1}^{N-1} \inf_{\pi_i} \mathbb{E}_{\pi_i} \left[ \|\mathbf{X}(t_i^1) - \hat{\mathbf{X}}(t_i^1)\|_2^2 \right] (t_i^1 - t_{i-1}^1) = \lim_{N \rightarrow \infty} \sum_{i=1}^{N-1} W_2^2(\mu(t_i^1), \hat{\mu}(t_i^1))(t_i^1 - t_{i-1}^1) \quad (71)$$

exists. This completes the proof of Theorem 3.

## Appendix E. Definition of different loss metrics used in the examples

Six loss functions for 1D cases were considered:

1. The squared Wasserstein-2 distance (Eq. (17))

$$W_2^2(\mu_N^e, \hat{\mu}_N^e),$$

where  $\mu_N^e$  and  $\hat{\mu}_N^e$  are the empirical distributions of the vector  $(X(t_1), \dots, X(t_{N-1}))$  and  $(\hat{X}(t_1), \dots, \hat{X}(t_{N-1}))$ , respectively. It is estimated by

$$W_2^2(\mu_N^e, \hat{\mu}_N^e) \approx \text{ot.emd2} \left( \frac{1}{M} \mathbf{I}_M, \frac{1}{M} \mathbf{I}_M, \mathbf{C} \right), \quad (72)$$

where `ot.emd2` is the function for solving the earth movers distance problem in the `ot` package of Python,  $M$  is the number of ground-truth and predicted trajectories,  $\mathbf{I}_\ell$  is an  $M$ -dimensional vector whose elements are all 1, and  $\mathbf{C} \in \mathbb{R}^{M \times M}$  is a matrix with entries  $(\mathbf{C})_{ij} = (X_N^i - \hat{X}_N^j)_2^2$ .  $X_N^i$  is the vector of the values of the  $i^{\text{th}}$  ground-truth trajectory at time points  $t_1, \dots, t_{N-1}$ , and  $\hat{X}_N^j$  is the vector of the values of the  $j^{\text{th}}$  predicted trajectory at time points  $t_1, \dots, t_{N-1}$ .

2. The squared time-decoupled Wasserstein-2 distance averaged over each time step (Eq. (18)):

$$\tilde{W}_2^2(\mu_N, \hat{\mu}_N) = \sum_{i=1}^{N-1} W_2^2(\mu_N^e(t_i), \hat{\mu}_N^e(t_i)) \Delta t$$

, where  $\Delta t$  is the time step and  $W_2$  is the Wasserstein-2 distance between two empirical distributions  $\mu_N^e(t_i), \hat{\mu}_N^e(t_i)$ . These distributions are calculated by the samples of the trajectories of  $X(t), \hat{X}(t)$  at a given time step  $t = t_i$ , respectively.

3. Mean squared error (MSE) between the trajectories, where  $M$  is the total number of the ground-truth and prediction trajectories.  $X_{i,j}$  and  $\hat{X}_{i,j}$  are the values of the  $j^{\text{th}}$  ground-truth and prediction trajectories at time  $t_i$ , respectively:

$$\text{MSE}(X, \hat{X}) = \sum_{i=1}^N \sum_{j=1}^M (X_{i,j} - \hat{X}_{i,j})^2 \Delta t.$$

4. The sum of squared distance between mean trajectories and absolute distance between trajectories, which is a common practice for estimating the parameters of an SDE. Here  $M$  and  $X_{i,j}$  and  $\hat{X}_{i,j}$  have the same meaning as in the MSE definition.  $\text{var}(X_i)$  and  $\text{var}(\hat{X}_i)$  are the variances of the empirical distributions of  $X(t_i), \hat{X}(t_i)$ , respectively. We shall denote this loss function by

$$(\text{mean}^2 + \text{var})(X, \hat{X}) = \sum_{i=1}^N \left[ \left( \frac{1}{n} \sum_{j=1}^M X_{i,j} - \frac{1}{n} \sum_{j=1}^M \hat{X}_{i,j} \right)^2 + \left| \text{var}(X_i) - \text{var}(\hat{X}_i) \right| \right] \Delta t.$$

5. Negative approximate log-likelihood of the trajectories:

$$-\log \mathcal{L}(X|\sigma) = - \sum_{i=0}^{N-1} \sum_{j=1}^M \log \rho_{\mathcal{N}} \left[ \frac{X_{i+1,j} - X_{i,j} + f(X_{i,j}, t_i) \Delta t}{\sigma^2(X_{i,j}, t_i) \Delta t} \right],$$

where  $\rho_{\mathcal{N}}$  is the probability density function of the standard normal distribution and  $f(X_{i,j}, t_i), \sigma(X_{i,j}, t_i)$  are the ground-truth drift and diffusion functions in Eq. (1).  $M$  and  $X_{i,j}$  and  $\hat{X}_{i,j}$  have the same meaning as in the MSE definition.

6. MMD (maximum mean discrepancy) (Li et al., 2015):

$$\text{MMD}(X, \hat{X}) = \sum_{i=1}^N (\mathbb{E}_p[K(X_i, X_i)] - 2\mathbb{E}_{p,q}[K(X_i, \hat{X}_i)] + \mathbb{E}_q[K(\hat{X}_i, \hat{X}_i)]) \Delta t,$$

where  $K$  is the standard radial basis function (or Gaussian kernel) with multiplier 2 and number of kernels 5.  $X_i$  and  $\hat{X}_i$  are the values of the ground-truth and prediction trajectories at time  $t_j$ , respectively.

Five  $W_2$  distance based loss functions for the 2D SDE reconstruction problem Example 4 are listed as follows

1. 2D squared  $W_2$  loss

$$\sum_{i=1}^{N-1} \left( W_2^2(\mu_{N,1}(t_i), \hat{\mu}_{N,1}(t_i)) + W_2^2(\mu_{N,2}(t_i), \hat{\mu}_{N,2}(t_i)) \right) \Delta t$$

where  $\mu_{N,1}(t_i)$  and  $\hat{\mu}_{N,1}(t_i)$  are the empirical distributions of  $X_1, \hat{X}_1$  at time  $t_i$ , respectively. Also,  $\mu_{N,2}(t_i)$  and  $\hat{\mu}_{N,2}(t_i)$  are the empirical distributions of  $X_2, \hat{X}_2$  at time  $t_i$ , respectively.

2. Weighted sliced squared  $W_2$  loss

$$\sum_{i=1}^{N-1} \left( \sum_{k=1}^m \frac{N_k}{\sum_{\ell=1}^m N_\ell} W_2^2(\mu_{N,k}^s(t_i), \hat{\mu}_{N,k}^s(t_i)) \right) \Delta t$$

where  $\mu_{N,k}^s(t_i)$  is the empirical distribution for  $\sqrt{X_1(t_i)^2 + X_2(t_i)^2}$  such that the angle between the two vectors  $(X_1(t_i), X_2(t_i))$  and  $(1, 0)$  is in  $[\frac{2(k-1)\pi}{m}, \frac{2k\pi}{m})$ ;  $\hat{\mu}_{N,k}^s(t_i)$  is the empirical distribution for  $\sqrt{\hat{X}_1(t_i)^2 + \hat{X}_2(t_i)^2}$  such that the angle between the two vectors  $(\hat{X}_1(t_i), \hat{X}_2(t_i))$  and  $(1, 0)$  is in  $[\frac{2(k-1)\pi}{m}, \frac{2k\pi}{m})$ ;  $N_k$  is the number of predictions such that the angle between the two vectors  $(\hat{X}_1(t_i), \hat{X}_2(t_i))$  and  $(1, 0)$  is in  $[\frac{2(k-1)\pi}{m}, \frac{2k\pi}{m})$ .

3. The loss function Eq. (17)

$$W_2^2(\mu_N^e, \hat{\mu}_N^e),$$

where  $\mu_N^e$  and  $\hat{\mu}_N^e$  are the empirical distributions of the vector  $(\mathbf{X}(t_1), \dots, \mathbf{X}(t_{N-1}))$  and  $(\hat{\mathbf{X}}(t_1), \dots, \hat{\mathbf{X}}(t_{N-1}))$ , respectively. It is estimated by

$$W_2^2(\mu_N^e, \hat{\mu}_N^e) \approx \text{ot.emd2}\left(\frac{1}{M}\mathbf{I}_M, \frac{1}{M}\mathbf{I}_M, \mathbf{C}\right), \quad (73)$$

where  $\text{ot.emd2}$  is the function for solving the earth movers distance problem in the `ot` package of Python,  $M$  is the number of ground-truth and predicted trajectories,  $\mathbf{I}_\ell$  is an  $M$ -dimensional vector whose elements are all 1, and  $\mathbf{C} \in \mathbb{R}^{M \times M}$  is a matrix with entries  $(\mathbf{C})_{ij} = |\mathbf{X}_N^i - \hat{\mathbf{X}}_N^j|_2^2$ .  $\mathbf{X}_N^i$  is the vector of the values of the  $i^{\text{th}}$  ground-truth trajectory at time points  $t_1, \dots, t_{N-1}$ , and  $\hat{\mathbf{X}}_N^j$  is the vector of the values of the  $j^{\text{th}}$  predicted trajectory at time points  $t_1, \dots, t_{N-1}$ .

4. The right-hand side of Eq. (18). It is estimated by

$$\begin{aligned} & \sum_{i=1}^{N-1} \inf_{\pi_i} \mathbb{E}_{\pi_i} [|\mathbf{X}(t_i) - \hat{\mathbf{X}}(t_i)|_2^2] \Delta t \\ & \approx \sum_{i=1}^{N-1} W_2^2(\mu_N^e(t_i), \hat{\mu}_N^e(t_i)) \Delta t \approx \Delta t \sum_{i=1}^{N-1} \text{ot.emd2}\left(\frac{1}{M}\mathbf{I}_M, \frac{1}{M}\mathbf{I}_M, \mathbf{C}_i\right), \end{aligned} \quad (74)$$

where  $\mu_N^e(t_i), \hat{\mu}_N^e(t_i)$  are the empirical distribution of  $\mathbf{X}(t_i), \hat{\mathbf{X}}(t_i)$ , respectively, and  $\text{ot.emd2}$  is the function for solving the earth movers distance problem in the `ot` package of Python.  $M$  is the number of ground-truth and predicted trajectories, and  $\mathbf{I}_M$  is an  $\ell$ -dimensional vector whose elements are all 1. Here, the matrix  $\mathbf{C}_i \in \mathbb{R}^{M \times M}$

has entries  $(\mathbf{C}_i)_{sj} = \|\mathbf{X}^s(t_i) - \hat{\mathbf{X}}^j(t_i)\|_2^2$  for  $i = 1, \dots, N - 1$ .  $\mathbf{X}^s(t_i)$  is the vector of the values of the  $s^{\text{th}}$  ground-truth trajectory at the time point  $t_i$ , and  $\hat{\mathbf{X}}^j(t_i)$  is the vector of the values of the  $j^{\text{th}}$  predicted trajectory at the time point  $t_i$ .

5. MMD (maximum mean discrepancy) (Li et al., 2015):

$$\text{MMD}(\mathbf{X}, \hat{\mathbf{X}}) = \sum_{i=1}^N (\mathbb{E}_p[K(\mathbf{X}_i, \mathbf{X}_i)] - 2\mathbb{E}_{p,q}[K(\mathbf{X}_i, \hat{\mathbf{X}}_i)] + \mathbb{E}_q[K(\hat{\mathbf{X}}_i, \hat{\mathbf{X}}_i)]) \Delta t,$$

where  $K$  is the standard radial basis function (or Gaussian kernel) with multiplier 2 and number of kernels 5.  $\mathbf{X}_i$  and  $\hat{\mathbf{X}}_i$  are the values of the ground-truth and prediction trajectories at time  $t_j$ , respectively.

## Appendix F. Default training setting

Here we list the default training hyperparameters and gradient descent methods for each example in Table 1.

Loss	Example 1	Example 2	Example 3	Example 4
Gradient descent method	AdamW	AdamW	AdamW	AdamW
Learning rate	0.001	0.002	0.002	0.0005
Weight decay	0.005	0.005	0.005	0.005
Number of epochs	1000	2000	2000	2000
Number of samples	100	200	256	200
Hidden layers in $\Theta_1$	2	1	1	1
Neurons in each layer in $\Theta_1$	32	32	32	32
Hidden layers in $\Theta_2$	2	1	1	1
Activation function	tanh	ReLU	ReLU	ReLU
Neurons in each layer in $\Theta_2$	32	32	32	32
$\Delta t$	0.1	0.05	1	0.02

Table 1: Training settings for each example.

## Appendix G. Uncertainty in the initial condition

For reconstructing the CIR model Eq. (31) in Example 2, instead of using the same initial condition for all trajectories, we shall investigate the numerical performance of our proposed squared  $W_2$  distance loss when the initial condition is not fixed, but rather sampled from a distribution.

First, we construct an additional dataset of the CIR model to allow the initial value  $u_0 \sim \mathcal{N}(2, \delta^2)$ , with  $\delta^2$  ranging from 0 to 1, and  $\mathcal{N}$  stands for the 1D normal distribution.

We then train the model by minimizing Eq. (18) to reconstruct Eq. (31) with the same hyperparameters as in Example 2. The results are shown in Table 2, which indicate our proposed squared  $W_2$  loss function is rather insensitive to the “noise”, *i.e.*, the variance in the distribution of the initial condition.

Loss	$\delta$	Relative Errors in $f$	Relative Errors in $\sigma$	$N_{\text{repeats}}$
$W_2$	0.0	0.072 ( $\pm 0.008$ )	0.071 ( $\pm 0.023$ )	10
$W_2$	0.1	0.053 ( $\pm 0.008$ )	0.043 ( $\pm 0.016$ )	10
$W_2$	0.2	0.099 ( $\pm 0.007$ )	0.056 ( $\pm 0.019$ )	10
$W_2$	0.3	0.070 ( $\pm 0.014$ )	0.083 ( $\pm 0.026$ )	10
$W_2$	0.4	0.070 ( $\pm 0.014$ )	0.078 ( $\pm 0.040$ )	10
$W_2$	0.5	0.075 ( $\pm 0.013$ )	0.138 ( $\pm 0.021$ )	10
$W_2$	0.6	0.037 ( $\pm 0.018$ )	0.069 ( $\pm 0.017$ )	10
$W_2$	0.7	0.075 ( $\pm 0.016$ )	0.043 ( $\pm 0.014$ )	10
$W_2$	0.8	0.041 ( $\pm 0.012$ )	0.079 ( $\pm 0.023$ )	10
$W_2$	0.9	0.082 ( $\pm 0.015$ )	0.108 ( $\pm 0.033$ )	10
$W_2$	1.0	0.058 ( $\pm 0.024$ )	0.049 ( $\pm 0.025$ )	10

Table 2: Reconstructing the CIR model Eq. (31) when  $u_0 \sim \mathcal{N}(2, \delta^2)$  with different variance  $\delta^2$ . The results indicate that the reconstruction results are not sensitive to the variance in the distribution of the initial value  $u_0$ .

## Appendix H. Neural network structure

We examine how the neural network structure affects the reconstruction of the CIR model Eq. (31) in Example 2. We vary the number of layers and the number of neurons in each layer (the number of neurons are set to be the same in each hidden layer), and the results are shown in Table 3.

The results in Table 3 show that increasing the number of neurons in each layer improves the reconstruction accuracy in  $\sigma$ . For the reconstructing CIR model in Example 2, using 32 neurons in each layer seems to be sufficient. On the other hand, when each layer contains 32 neurons, the number of hidden layers in the neural network seems does not affect the reconstruction accuracy of  $f, \sigma$ , and this indicates even 1 or 2 hidden layers are sufficient for the reconstruction of  $f, \sigma$ . Thus, reconstructing the CIR model in Example 2 using our proposed squared  $W_2$  based loss function does not require using complex deep or wide neural networks.

We also consider using the ResNet neural network structure (He et al., 2016). However, the application of the ResNet technique does not improve the reconstruction accuracy of the CIR model in Example 2. This is because simple feedforward multilayer neural network

Table 3: Reconstructing the CIR model when using neuron networks of different widths and numbers in each hidden layer to parameterize  $\hat{f}, \hat{\sigma}$  in Eq. (2).

Loss	Width	Layer	Relative Errors in $f$	Relative Errors in $\sigma$	$N_{\text{repeats}}$
$W_2$	16	1	0.131( $\pm 0.135$ )	0.170( $\pm 0.102$ )	10
$W_2$	32	1	0.041( $\pm 0.008$ )	0.109( $\pm 0.026$ )	10
$W_2$	64	1	0.040( $\pm 0.008$ )	0.104( $\pm 0.019$ )	10
$W_2$	128	1	0.040( $\pm 0.008$ )	0.118( $\pm 0.019$ )	10
$W_2$	32	2	0.049( $\pm 0.015$ )	0.123( $\pm 0.020$ )	10
$W_2$	32	3	0.094( $\pm 0.013$ )	0.166( $\pm 0.041$ )	10
$W_2$	32	4	0.124( $\pm 0.020$ )	0.185( $\pm 0.035$ )	10
$W_2$	32	5	0.041( $\pm 0.008$ )	0.122( $\pm 0.024$ )	10
$W_2$	32	6	0.043( $\pm 0.013$ )	0.117( $\pm 0.024$ )	10
$W_2$	32	7	0.044( $\pm 0.012$ )	0.109( $\pm 0.017$ )	10

Table 4: Reconstructing the CIR model Eq. (31) when neuron networks have different numbers of hidden layers and are equipped with the ResNet technique. Each hidden layer contains 32 neurons.

Loss	Layer	Relative Errors in $f$	Relative Errors in $\sigma$	$N_{\text{repeats}}$
$W_2$	1	0.045( $\pm 0.012$ )	0.116( $\pm 0.025$ )	10
$W_2$	2	0.053( $\pm 0.011$ )	0.108( $\pm 0.024$ )	10
$W_2$	3	0.071( $\pm 0.017$ )	0.117( $\pm 0.040$ )	10
$W_2$	4	0.096( $\pm 0.035$ )	0.149( $\pm 0.064$ )	10

structure can work well for learning Eq. (31) when reconstructing both  $f$  and  $\sigma$  so we do not need deep neural networks. Thus, the ResNet technique is not required. The results are shown in Table 4.

### Appendix I. Using the stochastic gradient descent method for optimization

Here, we shall reconstruct the OU process Eq. (32) in Example 3 with the initial condition  $X(0) = 0$  using the MMD and our squared  $W_2$  distance loss functions Eqs. (17) and (18) with different numbers of ground-truth trajectories and different batch sizes for applying the stochastic gradient descent technique for optimizing the parameters in the neural networks for reconstructing the SDE.

Table 5: Errors and runtime for different loss functions and different numbers of ground-truth trajectories when the training batch size is fixed to 16 and 256. The MMD and our proposed squared  $W_2$  distance Eq. (17) and well as our proposed time-decoupled squared  $W_2$  distance Eq. (18) are used as the loss function.

Loss	$N_{\text{sample}}$	Batch size	Relative error in $f$	Relative error in $\sigma$	Runtime	$N_{\text{repeats}}$
MMD	64	16	$0.30 \pm 0.12$	$0.49 \pm 0.17$	$1.19 \pm 0.59$	10
MMD	128	16	$0.30 \pm 0.09$	$0.50 \pm 0.20$	$1.27 \pm 0.58$	10
MMD	256	16	$0.31 \pm 0.09$	$0.44 \pm 0.21$	$1.31 \pm 0.59$	10
MMD	512	16	$0.22 \pm 0.12$	$0.43 \pm 0.18$	$1.22 \pm 0.37$	10
MMD	1024	16	$0.23 \pm 0.11$	$0.37 \pm 0.24$	$1.70 \pm 0.47$	10
Eq. (17)	64	16	$0.28 \pm 0.06$	$0.66 \pm 0.11$	$0.83 \pm 0.26$	10
Eq. (17)	128	16	$0.24 \pm 0.07$	$0.68 \pm 0.11$	$0.73 \pm 0.18$	10
Eq. (17)	256	16	$0.25 \pm 0.07$	$0.66 \pm 0.09$	$0.67 \pm 0.14$	10
Eq. (17)	512	16	$0.23 \pm 0.06$	$0.68 \pm 0.09$	$0.75 \pm 0.16$	10
Eq. (17)	1024	16	$0.25 \pm 0.07$	$0.66 \pm 0.09$	$1.02 \pm 0.47$	10
Eq. (18)	64	16	$0.20 \pm 0.06$	$0.42 \pm 0.08$	$0.61 \pm 0.14$	10
Eq. (18)	128	16	$0.22 \pm 0.06$	$0.37 \pm 0.14$	$0.78 \pm 0.35$	10
Eq. (18)	256	16	$0.21 \pm 0.07$	$0.39 \pm 0.16$	$0.88 \pm 0.46$	10
Eq. (18)	512	16	$0.23 \pm 0.06$	$0.43 \pm 0.15$	$0.72 \pm 0.11$	10
Eq. (18)	1024	16	$0.21 \pm 0.03$	$0.36 \pm 0.12$	$1.08 \pm 0.52$	10
MMD	64	256	$0.26 \pm 0.12$	$0.41 \pm 0.20$	$1.54 \pm 0.66$	10
MMD	128	256	$0.25 \pm 0.14$	$0.40 \pm 0.23$	$1.82 \pm 0.78$	10
MMD	256	256	$0.25 \pm 0.12$	$0.35 \pm 0.21$	$3.68 \pm 1.31$	10
MMD	512	256	$0.23 \pm 0.14$	$0.37 \pm 0.23$	$3.45 \pm 1.50$	10
MMD	1024	256	$0.23 \pm 0.13$	$0.35 \pm 0.21$	$3.09 \pm 1.35$	10
Eq. (17)	64	256	$0.28 \pm 0.08$	$0.61 \pm 0.04$	$1.19 \pm 0.45$	10
Eq. (17)	128	256	$0.31 \pm 0.07$	$0.61 \pm 0.07$	$1.04 \pm 0.48$	10
Eq. (17)	256	256	$0.26 \pm 0.07$	$0.53 \pm 0.03$	$0.96 \pm 0.43$	10
Eq. (17)	512	256	$0.26 \pm 0.08$	$0.56 \pm 0.05$	$0.98 \pm 0.40$	10
Eq. (17)	1024	256	$0.27 \pm 0.08$	$0.56 \pm 0.05$	$0.89 \pm 0.36$	10
Eq. (18)	64	256	$0.24 \pm 0.08$	$0.41 \pm 0.13$	$1.39 \pm 0.53$	10
Eq. (18)	128	256	$0.26 \pm 0.11$	$0.37 \pm 0.17$	$1.36 \pm 0.61$	10
Eq. (18)	256	256	$0.20 \pm 0.08$	$0.31 \pm 0.16$	$1.72 \pm 0.73$	10
Eq. (18)	512	256	$0.25 \pm 0.11$	$0.38 \pm 0.20$	$1.67 \pm 0.73$	10
Eq. (18)	1024	256	$0.26 \pm 0.10$	$0.39 \pm 0.20$	$1.64 \pm 0.79$	10

We train 2000 epochs with a learning rate 0.001 for all numerical experiments. In all cases, the loss functions converge before 2000 epochs. From Table 5, for all three loss function, *i.e.*, the MMD loss, Eq. (17), and Eq. (18), a larger number of training samples leads to more accurate reconstruction of  $\sigma$  (the noise term). Furthermore, it can be seen from Table 5 that using a smaller batch size (16) for training tends to lead to less accurate reconstruction of  $\sigma$  for the MMD and Eq. (17) loss functions even if the number of trajectories in the training set is large. This feature might arise because the trajectories are intrinsically noisy and evaluating MMD and Eq. (17) will be inaccurate if the batch size is small. Therefore, using a smaller batch size does not remedy the high cost of MMD as the reconstruction error is large and leads to inaccurate reconstruction of the ground-truth SDE for smaller  $N_{\text{sample}}$ . On the other hand, our proposed time-decoupled squared  $W_2$  distance loss function Eq. (18) gives similar performance in reconstructing  $f, \sigma$  for both a batch size of 16 and a batch size of 256. In other words, using Eq. (18) is more robust to a smaller batch size. From Table 5, using a smaller batch size (16) leads to faster training. Thus, we can consider using Eq. (18) as the loss function together with a smaller batch size to boost training efficiency.

From the results in both Example 3 and Table 5, our proposed time-decoupled squared  $W_2$  distance Eq. (18) is faster and more efficient than the MMD method and Eq. (17), making it potentially most suitable among all three loss functions for reconstructing SDEs.

## Appendix J. Additional discussion on the loss functions Eqs. (17) and (18)

Here, we make an additional comparison between using Eq. (17) and Eq. (18) as loss functions in Example 4. We set the number of training samples to be 128 and other hyperparameters for training to be the same as those in Example 4, as detailed in Table 1. First, we minimize Eq. (17) and record Eq. (17) and Eq. (18) over training epochs. Next, we minimize Eq. (18) and record Eq. (17) and Eq. (18) over training epochs. The results are shown in Fig. 5.

From Fig. 5 (a), we can see that when minimizing Eq. (17), Eq. (17) is almost  $10^{0.5}$  times larger than Eq. (18). However, when minimizing Eq. (18), the values of Eq. (17) and Eq. (18) are close to each other (Fig. 5 (b)). In both cases, Eq. (18) converges to approximately  $10^{-1}$ . Interestingly, minimizing Eq. (18) leads to a smaller value of Eq. (17). This again implies that minimizing Eq. (18) can be more effective than minimizing Eq. (17) in Example 4. More analysis on Eq. (18) is needed to understand its theoretical properties and to compare the performances of minimizing Eq. (18) versus minimizing Eq. (17) from numerical aspects.

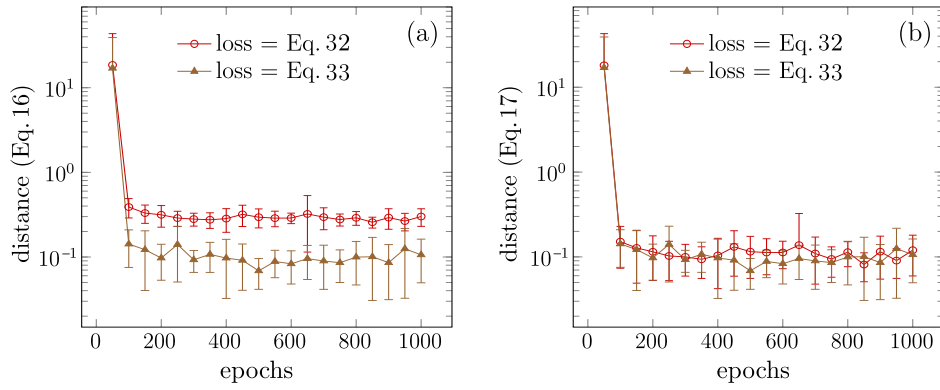


Figure 5: (a) The change in Eq. (17) and Eq. (18) when minimizing Eq. (17) over training epochs. (b) The change in Eq. (17) and Eq. (18) when minimizing Eq. (18) over training epochs.